AFRL-IF-RS-TR-2003-123
Final Technical Report
May 2003

HIGH PERFORMANCE LOCAL AREA NETWORKS

University of Maryland

Sponsored by
Defense Advanced Research Projects Agency
DARPA Order No. K208

APPROVED FOR PUBLIC RELEASE; DISTRIBUTION UNLIMITED.

AIR FORCE RESEARCH LABORATORY
INFORMATION DIRECTORATE
ROME RESEARCH SITE
ROME, NEW YORK

This report has been reviewed by the Air Force Research Laboratory, Information Directorate, Public Affairs Office (IFOIPA) and is releasable to the National Technical Information Service (NTIS). At NTIS it will be releasable to the general public, including foreign nations.

AFRL-IF-RS-TR-2003-123 has been reviewed and is approved for publication.

APPROVED: 

PAUL SIERAK
Project Engineer

FOR THE DIRECTOR: 

WARREN H. DEBANY, Jr., Technical Advisor
Information Grid Division
Information Directorate

REPORT DOCUMENTATION PAGE

Form Approved
OMB No. 074-0188

1. AGENCY USE ONLY (Leave blank)	2. REPORT DATE	3. REPORT TYPE AND DATES COVERED
	May 03	Final Aug 00 – Dec 02

4. TITLE AND SUBTITLE

HIGH PERFORMANCE LOCAL AREA NETWORKS

5. FUNDING NUMBERS

C - F30602-00-2-0617
PE - 62110E
PR - K208
TA - 03
WU - A1

6. AUTHOR(S)

Gary M. Carter

7. PERFORMING ORGANIZATION NAME(S) AND ADDRESS(ES)

University of Maryland
1000 Hilltop Circle
Baltimore, MD 21250

8. PERFORMING ORGANIZATION REPORT NUMBER

N/A

9. SPONSORING / MONITORING AGENCY NAME(S) AND ADDRESS(ES)

Defense Advanced Research Projects Agency
3701 North Fairfax Drive
Arlington, VA 22203-1714

AFRL/IFGA
525 Brooks Road
Rome, NY 13441-4505

10. SPONSORING / MONITORING AGENCY REPORT NUMBER

AFRL-IF-RS-TR-2003-123

11. SUPPLEMENTARY NOTES

AFRL Project Engineer: Paul Sierak, IFGA, 315-330-7346, sierakp@rl.af.mil

12a. DISTRIBUTION / AVAILABILITY STATEMENT

Approved for public release; distribution unlimited.

12b. DISTRIBUTION CODE

13. ABSTRACT ***(Maximum 200 Words)***

The potential use of optical switching to keep data in the optical domain will be used for the interconnection of local and metropolitan optical networks. Keeping data in the optical domain over various optical networks leads to new design challenges as the variability of path leads to a variability of impairments. This work accomplished experiments at 10, 20, and 40 Gbps on the ATDNET which is a metropolitan network. The optical domain impairments limited transmission rates to 20 Gbps. Polarization mode dispersion precluded 40 Gbps transmission. When ATDNET was connected to the BOSSNET, which is located in New England, dispersion allocation and polarization mode dispersion limited performance. A different optimization scheme for impairment reduction is required.

14. SUBJECT TERMS

fiber optic networks, single mode networks, polarization mode dispersion, signal impairment

15. NUMBER OF PAGES

41

16. PRICE CODE

17. SECURITY CLASSIFICATION OF REPORT	18. SECURITY CLASSIFICATION OF THIS PAGE	19. SECURITY CLASSIFICATION OF ABSTRACT	20. LIMITATION OF ABSTRACT
UNCLASSIFIED	UNCLASSIFIED	UNCLASSIFIED	UL

TABLE OF CONTENTS

LIST OF FIGURES

FINAL TECHNICAL REPORT
For
"High Performance Local Area Networks"
Air Force Contract #F30602-00-2-0617
UMBC—Professor Gary M. Carter, P.I.

I. Introduction

The research sponsored by this grant had a primary goal of investigating high performance all-optical networks. It was designed to address the suitability of optically connecting high data rate local and/or metropolitan area networks to long-haul high performance networks. The research was carried out on installed optical network test beds. One test bed used for this research is ATDNET which is a metropolitan area network around Washington, DC. The other test bed used in this research was BossNet, a long haul network. These two test beds were optically connected near Washington, DC. In addition supporting research was accomplished at UMBC in Professor Gary Carter's laboratories. The research addressed data transmission at 10, 20, and 40 Gigabits/sec over optical networks with the aim of quantifying the limitations on the transmission and where possible devising methods to overcome these limitations. The effects of noise, dispersion distribution, optical nonlinear effects in the transmission optical fiber, and polarization effects were investigated and will be reported on in the following sections. These sections will describe high speed transmitter and receiver configurations; laboratory experiments; network experiments, and conclusions. This will provide a comprehensive understanding of the results and their implications for all-optical networks.

To appreciate the necessity of this research it is important to note that installed fiber optic systems are point-to-point transmission systems. Laboratory systems have achieved impressive laboratory performance by optimizing a number of system parameters, but this optimization critically depends on the fiber type, optical amplifier spacing, dispersion distribution, data format, and optical channel spacing in a multi-wavelength system. These results have set criteria that are desirable for long-haul transmission systems. Local area networks have or are migrating to the optical domain with research concentrating of increasing data rates to 10 Gigabits/sec in the near future. Metropolitan area networks are migrating to 10 Gigabit/s rates. With the advent of relatively inexpensive optical cross-connect switches it is now possible to optically interconnect

nodes on networks. These devices currently switch entire channels with research looking into the possibility of optical packet switching. Using optical routers instead of electrical routers offers the possibility of tremendous cost savings for network providers. As a result if this technology is adopted in the future it is likely to make the optical technology more widely deployed and increase overall performance. The research issue addressed in this report concerns high performance local area networks and metropolitan area networks that could be optically interconnected to long haul networks. This introduces variability in the transmission path that can no longer be simply optimized from start to finish as is done in a point-to-point system. The data may be transported over portions of the network that are very different

II. High Speed Transmitters and Receivers

As part of this project both transmitters and receivers that could work at 10, 20, and 40 Gb/s needed to be developed. The main difficulty is in the receiver at rates greater than 10 Gb/s since the bit-error rate testers we use operate only up to 12.5 Gb/s. The data must be either demultiplexed electronically or optically down to the lower rate. As will be explained in the following optical demultiplexing was chosen.

The 10 Gb/s transmitter is shown schematically in Figure 1. It uses a cw laser which is modulated at the clock rate of 10 GHz to produce a train of pulses. The electro-optic transducer is an electro-absorption modulator (EAM) which produces pulse widths of approximately 20 ps when modulated at a 10 GHz rate. The data from a pattern generator is superimposed on the pulse train via an electro-optic modulator (EOM). The eye diagram of the data modulated with a pseudo-random bit sequence is shown in the inset in Figure 1.

To increase the data rate to higher rates the data was optically multiplexed as shown schematically in Figure 2. Here the modulated data at 10 Gb/s is incident on device that splits the light into two streams (conceptually a 3 dB splitter). One of the streams is delayed in time with respect to the other. The time delay between the streams must be a multiple of the bit period, 50 ps, for the new data rate, 20 Gb/s. This multiple must be at least 3 or larger to get a true 20 Gb/s data rate. For short delays the data between the two data streams is somewhat correlated. For most of the experiments this does not present a problem.

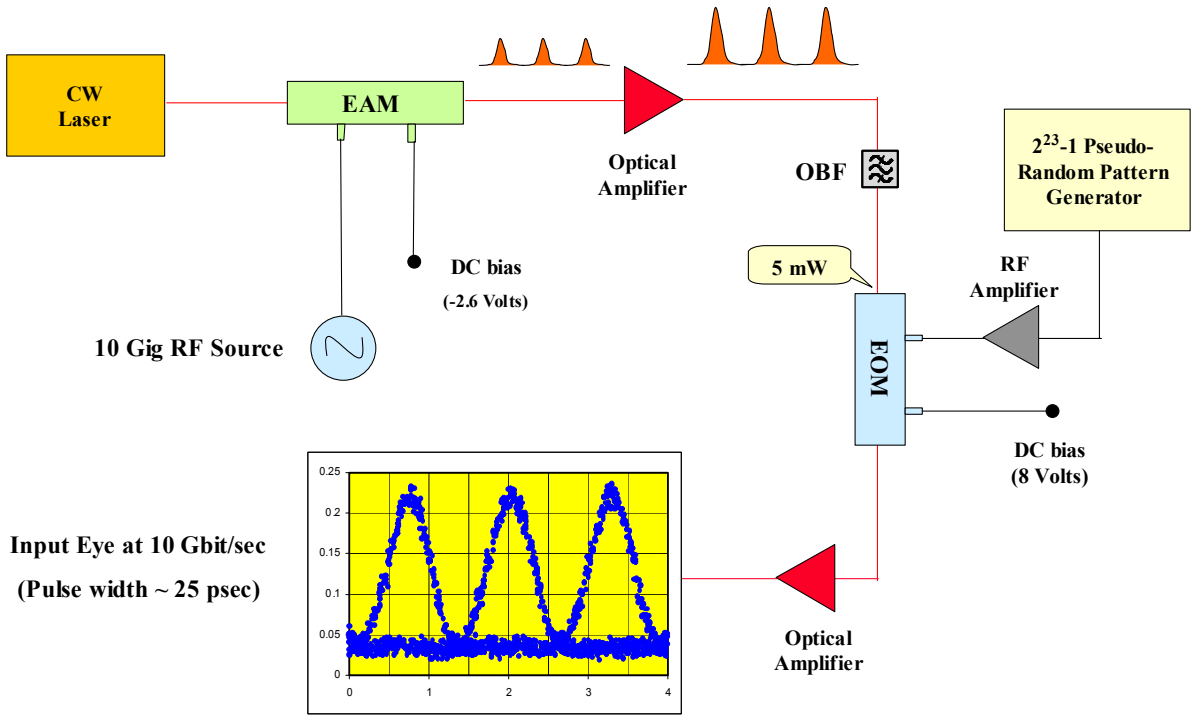

Figure 1. Schematic of 10 GHz RZ transmitter used in 10 Gigabit/sec experiments. The eye diagram is shown for the modulated data stream.

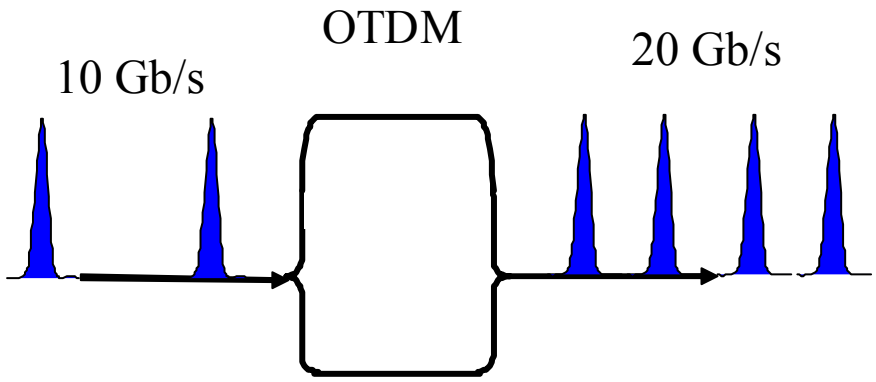

Figure 2. Optical time division multiplexing (OTDM) used to produce 20 Gb/s data stream from a 10 Gb/s data stream.

To increase the data rate to 40 Gb/s a two stage multiplexer was used as shown schematically in Figure 3. The key in these multiplexers is to build them so they are stable and low loss. It is important to note that 20 Gb/s data was obtained using he transmitter scheme shown in Figure 1. With the bit period being 50 psec in duration one needs short pulses to

prevent part of the energy of one bit from temporally overlapping adjacent bits. While the EAM source has worked it has been replaced with a modelocked fiber laser for 20 and 40 Gb/s experiments. We can produce pulses on the order of 5 to 10 ps with this laser which is driven by the master clock to produce a 10 GHz pulse train.

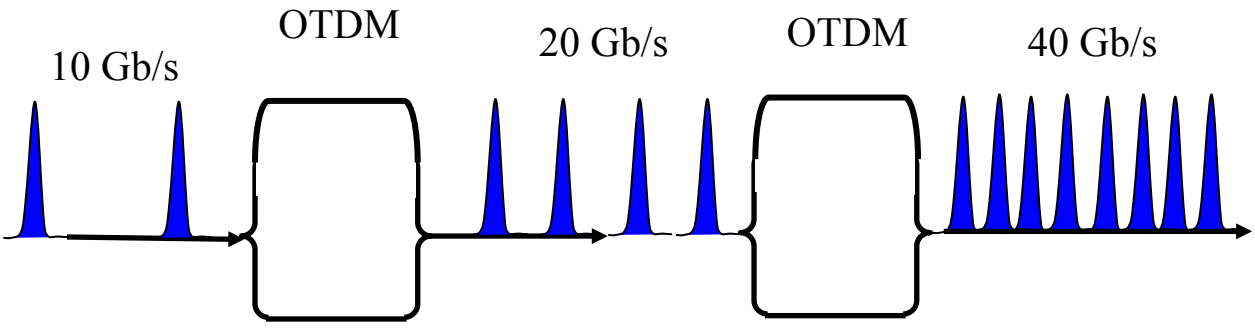

Figure 3. Optical time division multiplexing used to produce 40 Gb/s data stream from a 10 Gb/s data stream.

The major difficulty at the receiver is to develop a way to demultiplex the data down to lower rates for error and other measurements. An optical demuliplexing scheme was chosen as shown schematically in Figure 4. Here the data stream passes through an electro-absorption modulator. The data is split into a data stream and clock stream. The clock stream as shown in Figure 4 is detected by a high speed photo-detector and the photo-current is filtered by a 10 GHz clock (a narrow band electrical filter at the clock frequency of 10 GHz). The output from the clock is amplified and applied to the EAM. The signal to the EAM is a sinewave and is synchronized to the incoming data. Thus the EAM's transmission is high once per cycle and every other bit is highly attenuated due to the nonlinear transmission of the EAM. Note that an overall fixed time delay adjustment must be made due to the long length of RF cable between the photo-detector and the EAM. Also this is operating in a feedback mode.

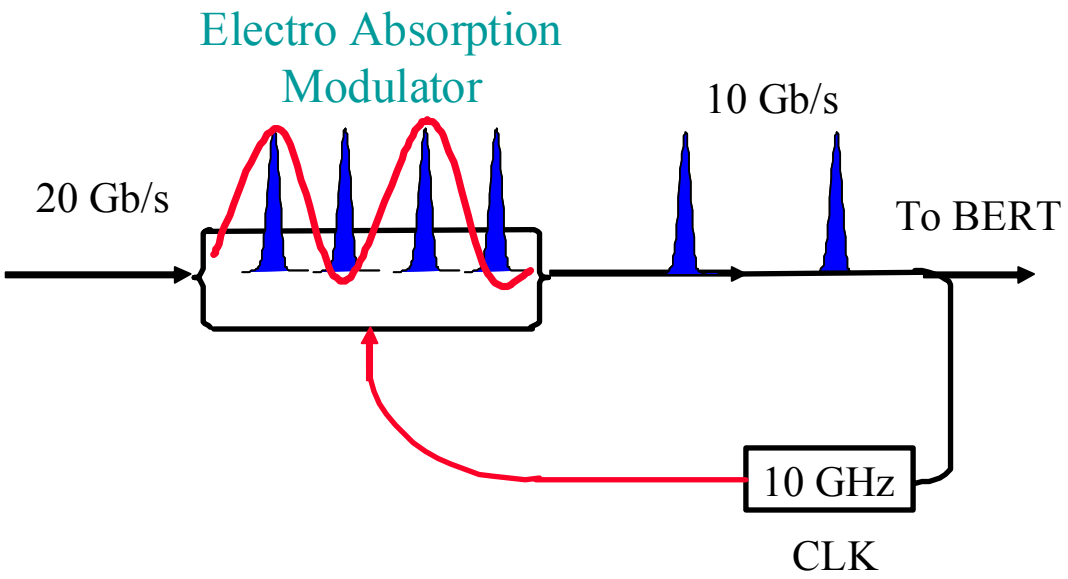

Figure 4. Schematic of demultiplexing scheme to extract a 10 Gb/s data stream from the 20 Gb/s input stream.

Figure 5 shows the schematic of the device used to demultiplex data down from 40 to 10 Gb/s. Note it is basically a dual stage of Figure 4 and a frequency doubler doubles the 10 GHz to 20 GHz. The initial experiments used an electro-optic modulator as the first stage since that was the only device initially available to this research program that could be modulated at 20 GHz. However this device is very polarization sensitive and thus worked in the network environment but the polarization state into the demultiplexer was frequently adjusted by using a polarization controller. Eventually a high speed EAM became available and the device shown in Figure 5 was realized.

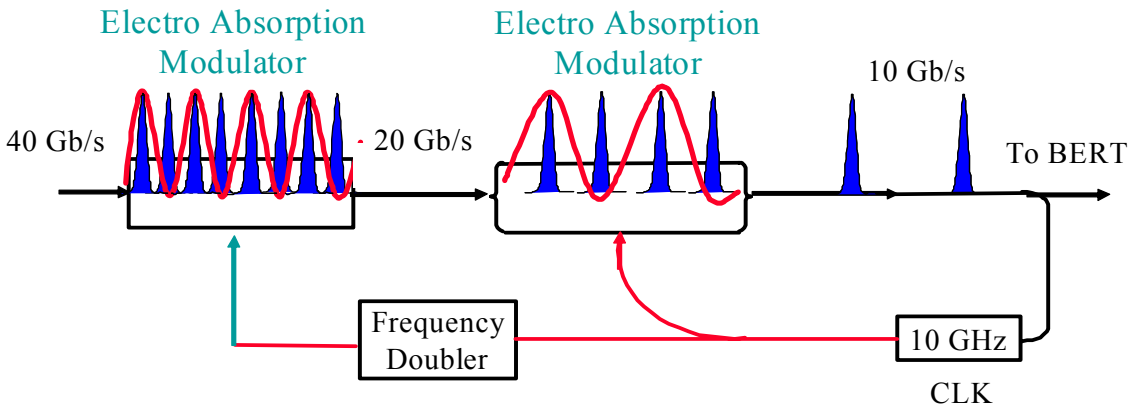

Figure 5. Dual stage demultiplexer to reduce data rate from 40 to 10 Gb/s.

These demultiplexers (demuxer) have been used extensively in laboratory experiments. The experiments have verified that the device is polarization independent in its operation. The slight polarization sensitivity of the EAM's does not affect the clock recovery and demuxing function significantly. Also these laboratory experiments show that this demuxer does not add any significant amount of timing jitter to the data. The 40 Gb/s laboratory experiments used a recirculating loop to experimentally emulate transmission over thousands of km. For distances up to 6400 km the only degradation attributable to the demultiplexer was time windowing for the data. No effects of additional timing jitter was observed [1]. The time windowing is predictable. This windowing is comparable to that measured with state-of-the-art electronic demultiplexers. The optical demultiplexing scheme is approximately one order of magnitude cheaper than the electronic versions.

III. Transmission Experiments

The transmission experiments were performed on installed networks. The first network used for this research is called ATDNET and is a government sponsored experimental metropolitan area network in the Washington, DC area linking a number of government facilities. This network used standard single mode fiber with a large dispersion (17 ps/nm-km). Thus any high speed experiments would require dispersion compensation fiber (DCF) to be placed at the transmitter and/or receiver. This research used the Laboratory for Telecommunication Sciences node on ATDNET. The transmitter and receiver were located there and the transmission experiments went out on one fiber and returned on a second fiber to the receiver.

One of the first set of high speed experiments was to transmit 20 Gb/s data stream from LTS to NASA and back for a round-trip distance of 41 km. It was necessary to use DCF fiber to compensate for the total dispersion in the 41 km which is approximately 700 ps/nm. Figure 6 shows the eye diagram at the input, i.e. before transmission and Figure 7 shows the data at the receiver after transmission. Both sets of eye diagrams shown are after demultipexing down to 10 Gb/s. The measured error rate was typically $\approx 1 \times 10^{-12}$. This error rate was typical for the measurements made also at 10 Gb/s using both return-to-zero (RZ) data formats (pulses) and non-return to zero (NRZ) data formats.

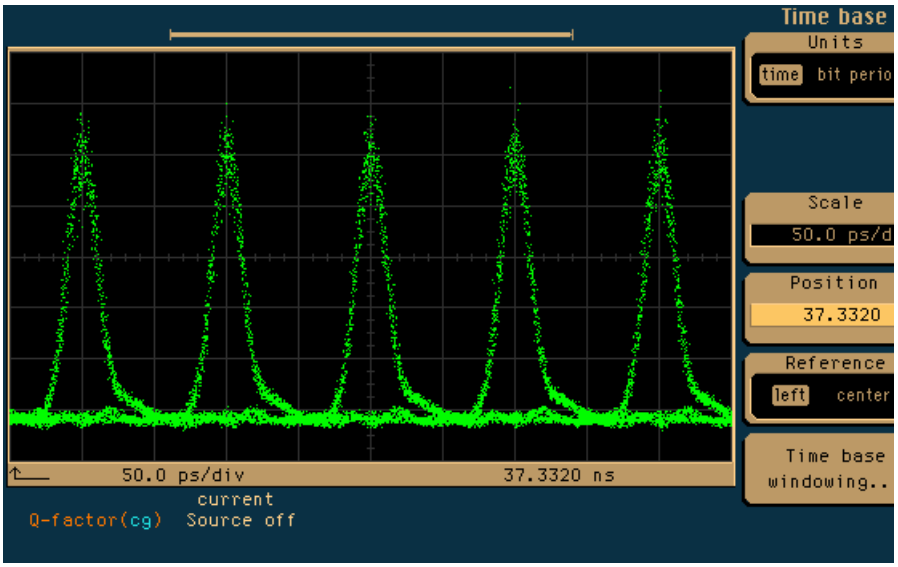

Figure 6. 20 Gigabit/sec data demultiplexed down to 10 Gigabit/sec. Data was taken at the transmitter.

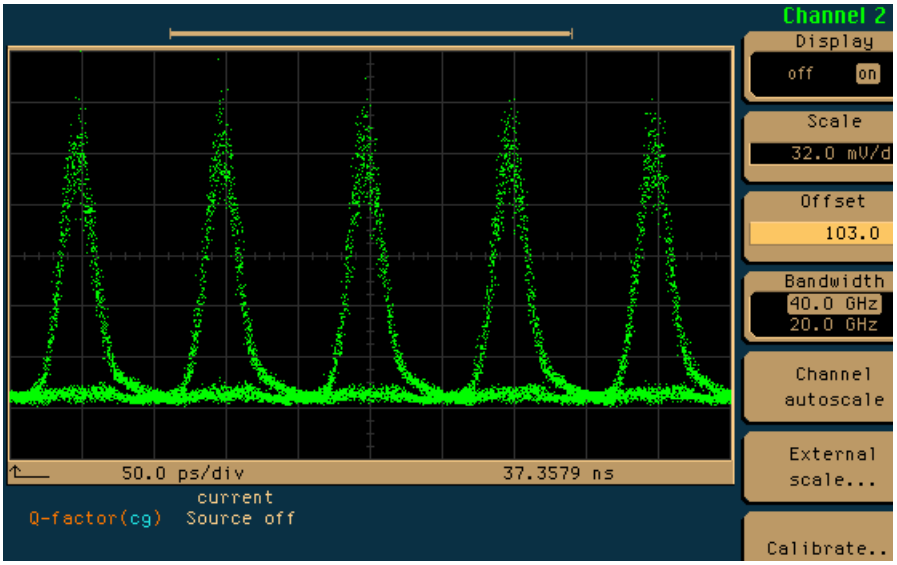

Figure 7. 20 Gigabit/sec data demultiplexed down to 10 Gigabit/sec at the receiver after propagating from LTS to NASA and back to LTS.

The cause of these infrequent errors is difficult to trace due to their infrequency. Similar error rates were reported by other researchers at LTS. This is an area that still must be investigated. However, the success of these experiments is a validation of the multiplexing and

demultiplexing schemes described in previous sections. Further, the RZ data format is ideal for long-haul transmission experiments that were planned for subsequent parts of this research.

The next stage of the research involved in connecting ATDNET to another network, BossNet which ran from the Washington, DC area to Boston, MA. The first part of this work consisted of making connections at ISI East, another node on ATDNET, located in Virginia. Components were used that were available for the connection resulting in excess loss. Although this limited the signal-to-noise ratios available, the performance was good enough to carry out experiments. BossNet is a different fiber type made up of much lower dispersion fiber and is dispersion compensated at each fiber amplifier location. The experiments transmitted data from LTS to either Wilmington, DE or New York (near NYC) and reception was at LTS. Figure 8 shows data from the 10 Gb/s experiments.

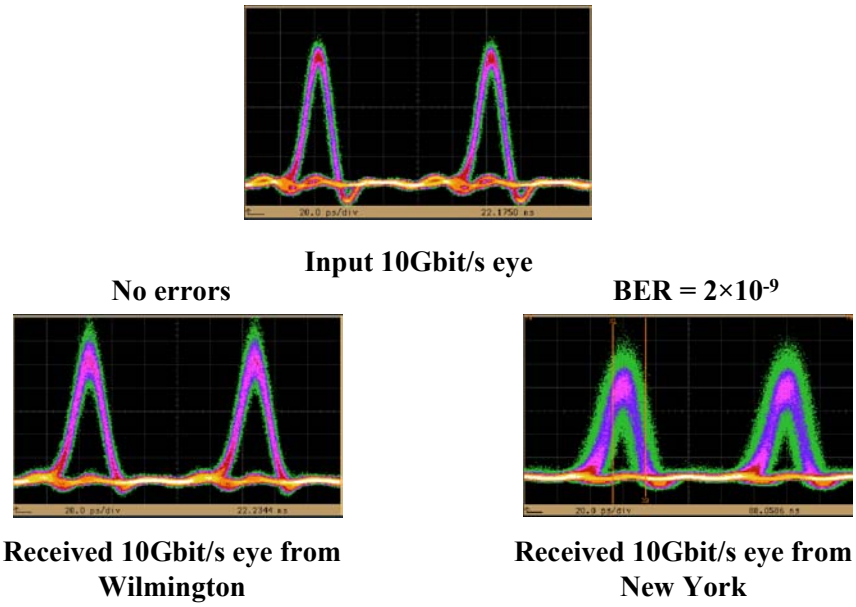

Figure 8. 10 Gb/s data for LTS to Wilmington and New York.

The error rate on the data to NY and back is clearly due to optical amplifier noise that is generated overcoming fiber and component losses. The RZ performance was excellent to Wilmington and back indicating that the experimental design worked well for these two networks

with very different fiber plants. 20 Gb/s experiments were attempted and the results to Wilmington and back are shown in Figure 9.

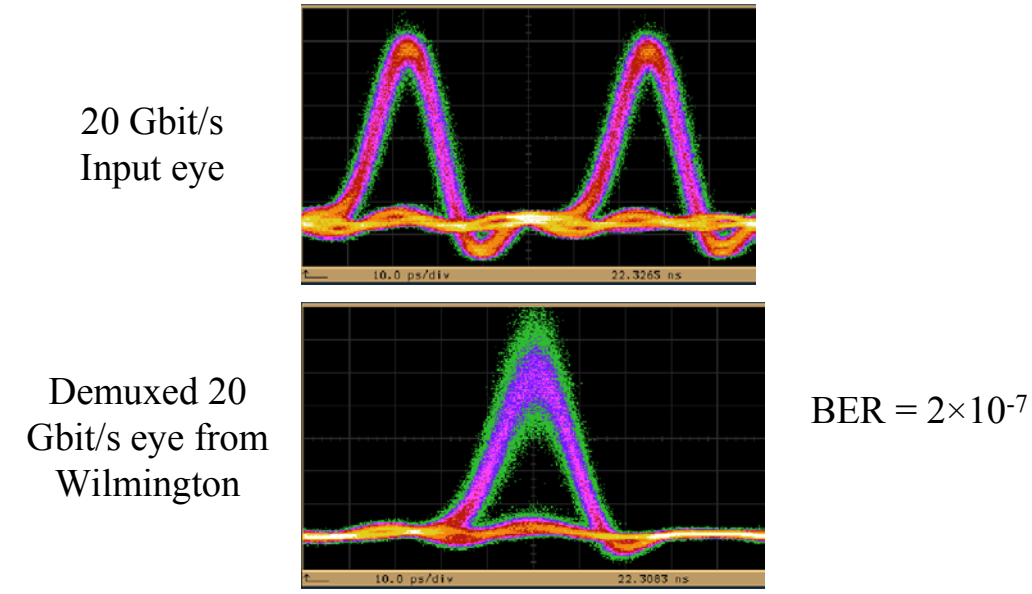

Figure 9. 20 Gb/s transmission from LTS to Wilmington, DE and back across both ATDNET and BossNet. The top eye diagram is at 20 Gb/s before demultiplexing and the received eye at the bottom is after demultiplexing.

These limitations at 20 Gb/s and at 10 Gb/s over longer distances are attributable to signal-to-noise. The data is summarized in Figure 10 which shows the Q measurements and timing jitter measurements made from the eye diagrams. The Q measurement is the ratio of difference of the means of the one and zero bits to the sum of their respective standard deviations. As the noise increases the standard deviations of the one and zero bits also increases. Typically the noise on the one bits is the dominant factor due to signal-spontaneous emission beat noise.

	10 Gbit/s Data		20 Gbit/s Data	
	Measured Q Factor	Timing Jitter (psec)	Measured Q Factor	Timing Jitter (psec)
LTS to Wilmington	9.55	1.39	6.69	1.45
LTS to New York	6.44	3.74	N/A	N/A

Figure 10. Q and timing jitter measurements at 10 and 20 Gb/s.

The large Q for the 10 Gb/s data to Wilmington and back indicates a low error rate. The Q to NY is approximately the value one would have for a BER of 10^{-9}. Note the timing jitter increases as well but the timing jitter would have to be in excess of 5 ps to limit the transmission at 10 Gb/s. The 20 Gb/s experiments show similar results to Wilmington. The timing jitter would have to exceed 2.5 ps to limit the transmission. The Q value is low indicating signal-to-noise is limiting the transmission. Note that the bit-error rate is somewhat smaller than that measured with a similar Q on the 10 Gb/s. This is consistent with the sensitivity of the measurements to error. A 20 % measurement error in Q (typical for these measurements) results in two order of magnitude change in error rate at these rates.

These results were obtained after optimization of the dispersion map. This optimization has profound implications of this for all-optical networks. Due to the ATDNET portion of the fiber it was necessary to add the DCF in to prevent pulse spreading. However, the exact location of this compensation makes a tremendous difference in the system performance. Figure 11 shows the effects of first lumping the compensation at the transmitter and then splitting it between the transmitter and receiver.

LTS – Wilmington

Pre-compensation

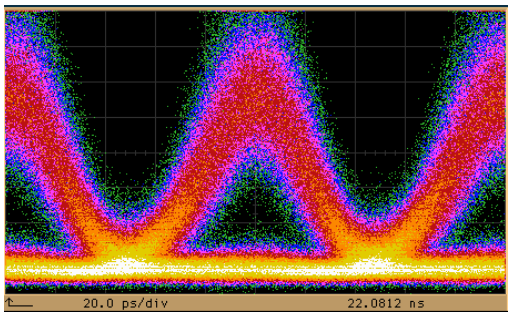

BER = 1×10^{-7}

LTS – Wilmington

Pre and Post compensation

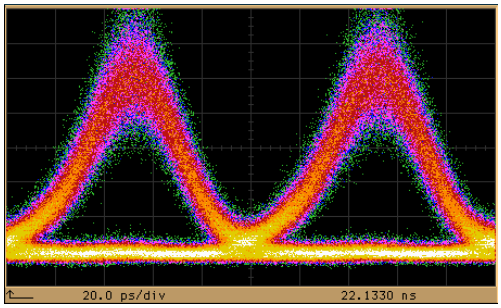

BER = 1×10^{-10}

Figure 11. The top eye diagram shows the results for the dispersion compensation being placed at the transmitter. The bottom eye diagram shows the improvements by splitting the compensation between the transmitter and receiver.

The higher bit-error rate in Figure 11 is due to timing jitter as can be seen from the width of the lines. The timing jitter is greatly reduced by splitting the compensation. This excess timing jitter is due to nonlinear optical interactions between adjacent pulses in the bit stream. The pulses overlap temporally due to the dispersion for portions of the network. While they are overlapped the pulses interact in the fiber through the nonlinear optical response of the fiber. This results in frequency shifts for the adjacent pulses. These frequency shifts of pulses relative to each other results in timing jitter in the presence of dispersion.

This realization came from extensive laboratory work using a recirculating loop to transmit data long distances. This WDM loop was located at UMBC and had similar transmission characteristics as that found in ATDNET and BossNet. The dispersion was compensated every 50 to 75 km. The losses were controlled in the laboratory so the transmission distances achieved were quite long. Figure 12 shows 10 Gb/s data transmitted over 5,000 km. The eye diagram is almost closed due to timing jitter. The accumulated dispersion zig-zags but is always above zero and progressively increases. The final compensation is in the receiver to make

the total dispersion zero at the receiver. For comparison the same experiment was performed by readjusting the dispersion compensation. Some of the compensation was added at the transmitter to yield a symmetric dispersion compensation accumulation as can be seen in Figure 13. This symmetry is the key to the successful results as can be seen from the clean eye diagram with low timing jitter in Figure 13 [2]. This conclusion is backed up by theoretical modeling. While this optimization was used in experiments represented by Figure 11 the data in Figure 12 and 13 indicates that this represents a problem for optically connected networks. Note that to truly optimize the accumulated dispersion to make it symmetric about zero requires knowing the transmission distance. In an active network, optical switches will re-route data over different portions of the network or onto other networks. Thus the transmission distance will vary depending on the network configuration. Further some portions of a network may or may not be compensated. This degree of variability will make it imperative to have the network management system have some knowledge of the transmission route upon switching. Further the management system will need the ability to adjust dispersion at the transmitter and receiver to obtain the required performance.

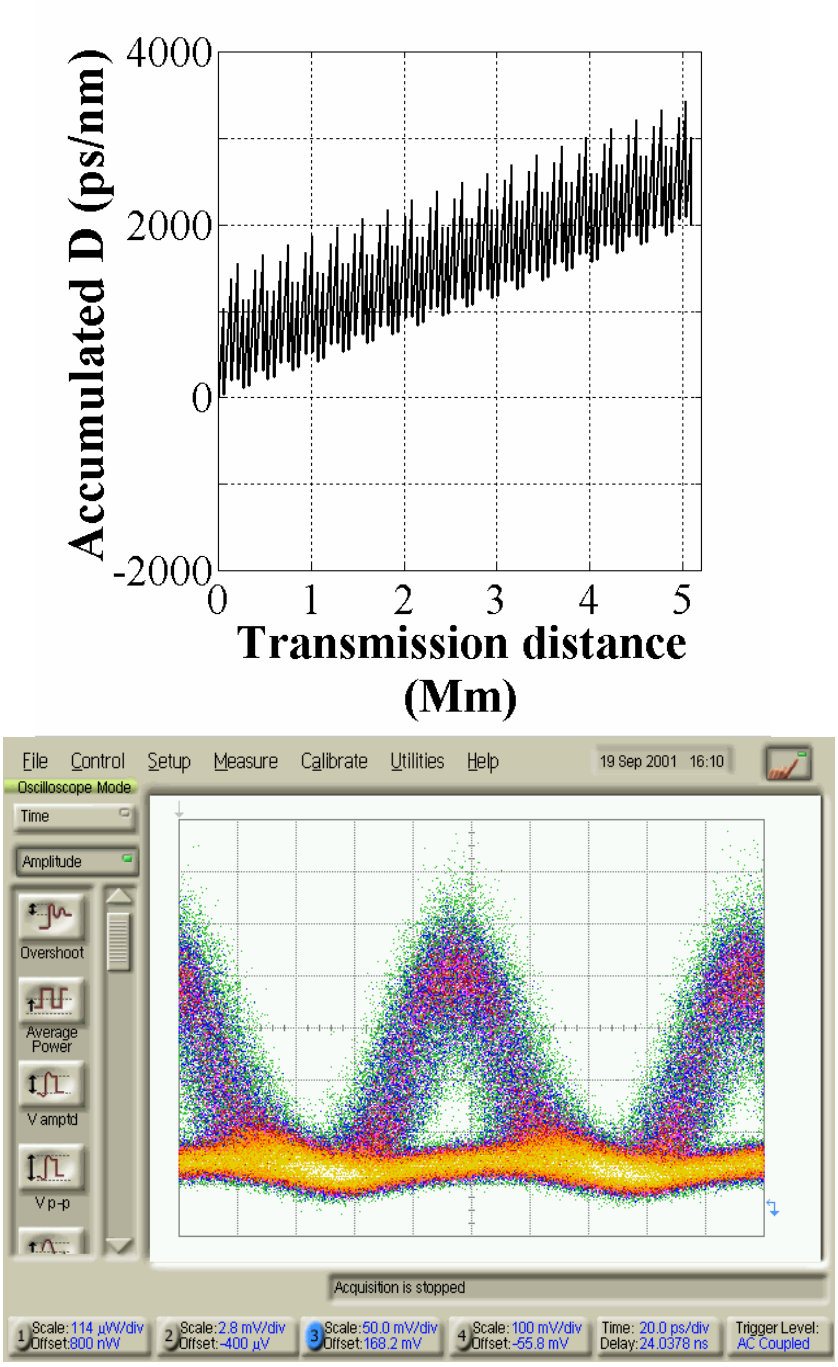

Figure 12. Accumulated dispersion and eye diagram for 10 Gb/s RZ laboratory experiment over long distances. Note the eye diagram is taken at 5,000 km.

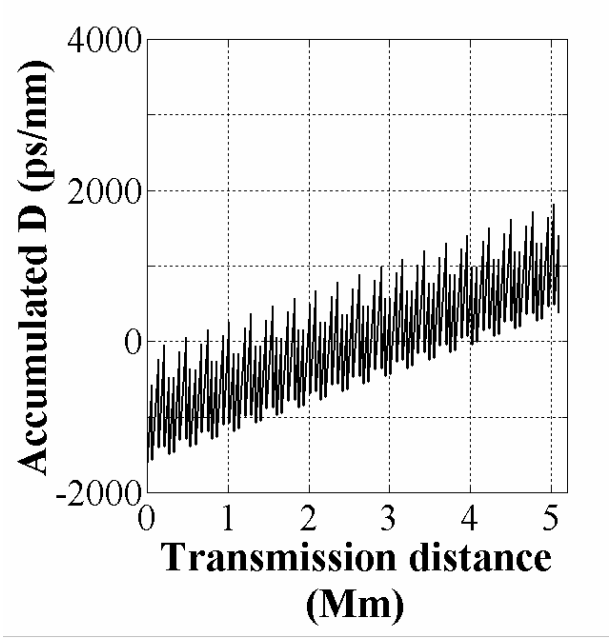

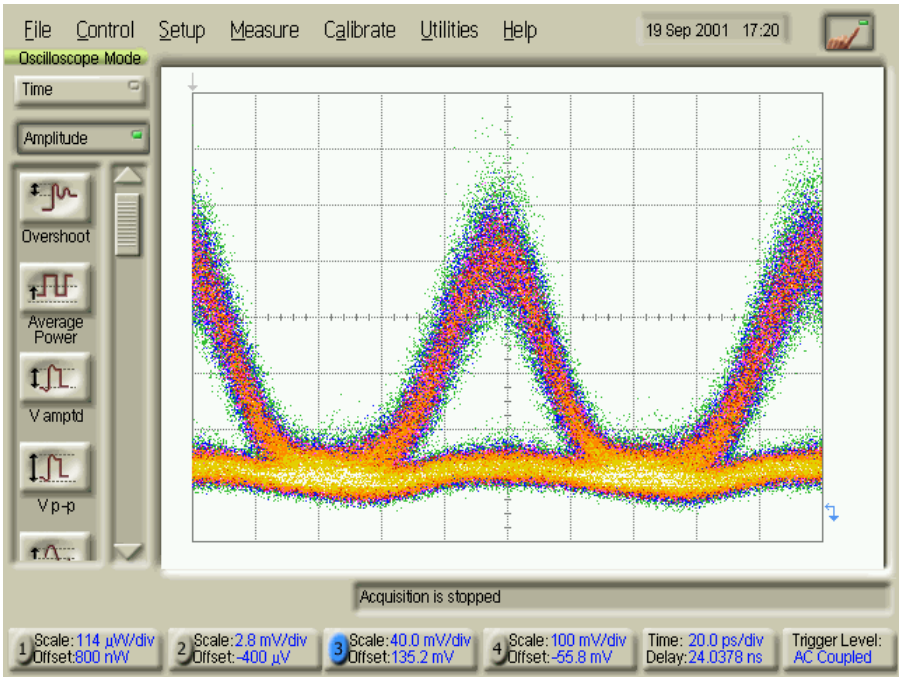

Figure 13. Accumulated dispersion and eye diagram for 10 Gb/s RZ laboratory experiment over long distances. Note the improved eye diagram taken at 5,000 km due to the symmetric accumulated dispersion around zero.

Experiments at 40 Gb/s were attempted on ATDNET but failed. The transmission performance seemed to depend dramatically on the polarization of the transmitted data. This led to a fruitful investigation of polarization effects in the network due to polarization dependent loss (PDL) and polarization mode dispersion (PMD). These affects are well known to limit data transmission at higher data rates. In particular one can understand the limitation due to PMD by noting that the birefringence of the fiber can cause the pulse to split into two polarization states. Each polarization state travels at a slightly different velocity and hence the two states develop a relative time shift [3]. When detected in a photo-detector the pulses are now broadened. If this relative time delay is large the part of the broadened pulse shows up in the next time slot and hence one gets inter-symbol interference. This is a source of errors. This has been studied in the laboratory as part of this research and the effect is visible in modern fibers if the data travels thousands of kilometers. However, older fibers have a larger effect and thus PMD can be seen over shorter distances. A study of the PMD and the PDL in ATDNET was initiated by the UMBC research team with Dr. Chris Richardson from the University of Maryland College Park.

The PMD measured in ATDNET is time varying because of the orientation of the birefringence changes with time due to changing stress and temperature. The effect that was measured is called the differential group delay or DGD which is a measure of the time separation between the two polarization states. A typical plot of this is shown in Figure 14. The distribution is taken over several days. Thus while the mean DGD is small relative to a 100 ps time slot, it becomes significant for a 50 ps time slot appropriate for 20 Gb/s. Note that there are some points that would yield a delay of over 30 ps enough to cause errors at 20 Gb/s given the finite pulse width. Also these values are large compared to the 25 ps time window for 40 Gb/s window. Thus this data confirms that the fiber in ATDNET is a significant problem. Figure 15 shows the time variation for the data shown in Figure 14. These bursts of DGD show the complexity of the problem. Typical models and laboratory experiments average over time to get smooth looking distributions for the DGD. However, errors will occur when the DGD is large and happen for short periods of time. If one knows the time scale of the randomization then these pdf's can be used to predict outage probabilities. However, detailed and ongoing experiments on ATDNET show that the DGD can apparently spike due to external forcing functions like wind velocity. This cannot be modeled in an average statistical sense. Note that in Figure 16 the measured DGD

on a different portion of ATDNET is double humped. Thus the distributions are not the same across all of the network [4].

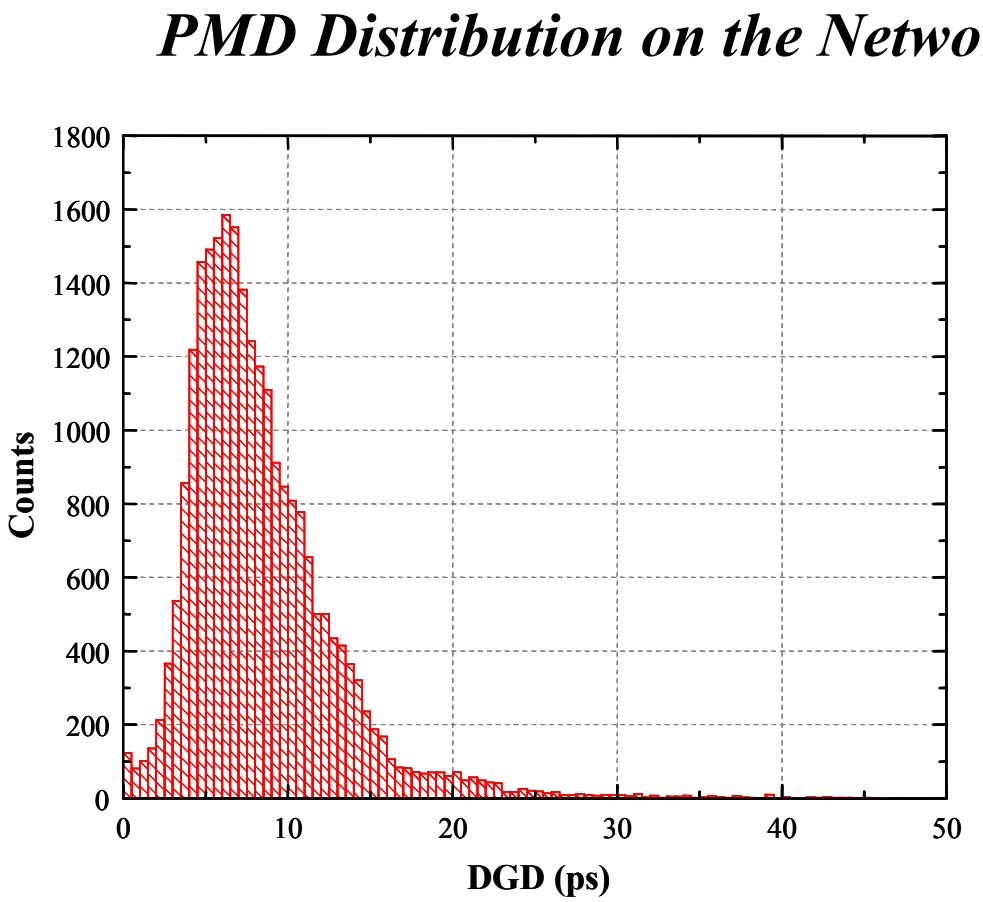

Figure 14. Measured DGD on ATDNET.

It is the variability that makes the characterization of the PMD for system design difficult. A network then can be a concatenation of a number of segments with different polarization behaviors. Note in Figure 17 we show the measured DGD for going from LTS to NYC and back to LTS. Thus the fiber encountered is the ATDNET and BossNet fiber. Note that the fiber in Figure 16 is part of the segments in the connections used in obtaining the data in Figure 17. Thus the statistics of the whole look different that the parts. At this moment there is no simple way to analyze this. This is a very fruitful and important new area of research.

Polarization dependent loss (PDL) is also an issue in networks. Optical switches, couplers, isolators, wavelength multiplexers and demultiplexers all have preferential loss along some axis

relative to an orthogonal axis. These losses are typically a few tenths of dB but the random nature of the birefringence of the fiber can cause these effects to add up. A series of experiments were carried out on PDL on BossNet and ATDNET.

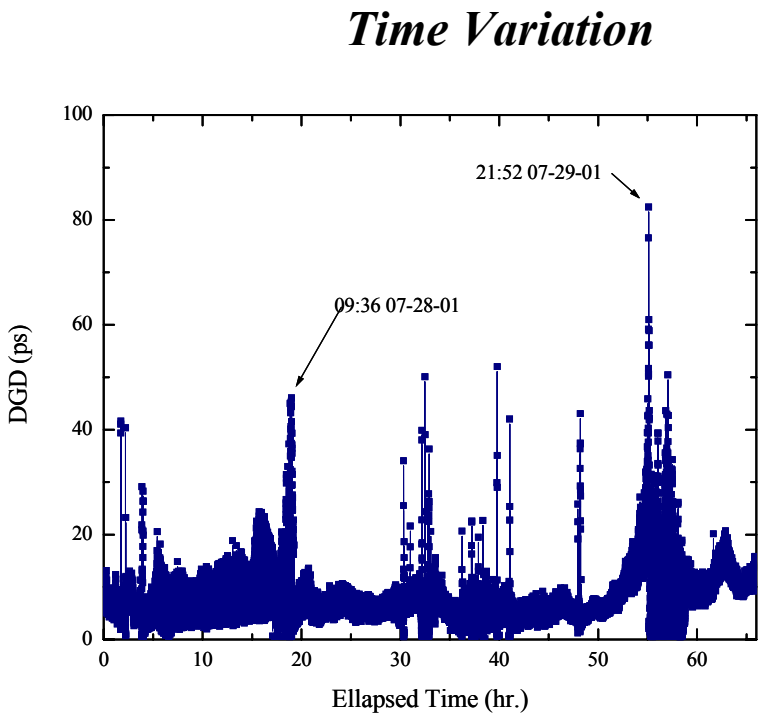

Figure 15. Measured DGD on ATDNET as a function of time.

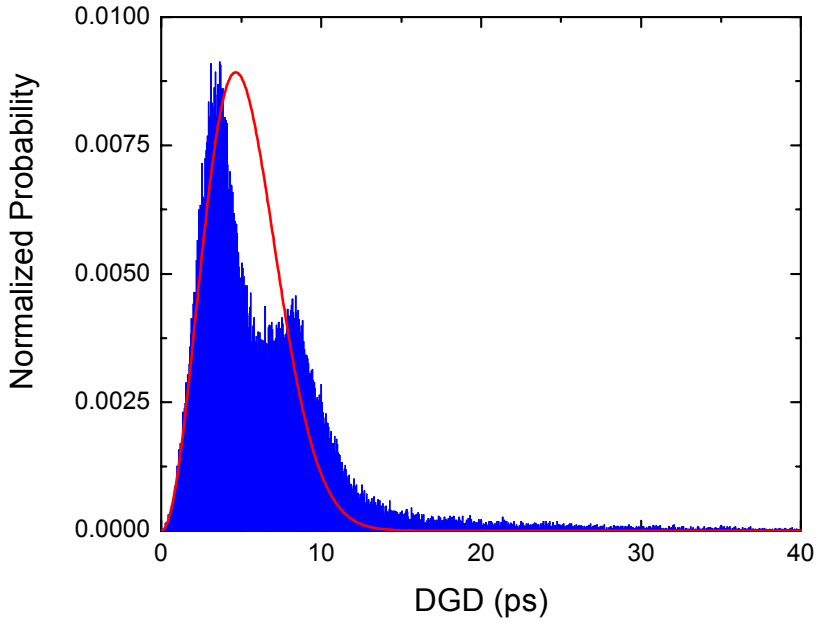

Figure 16. Measured DGD on a second portion of ATDNET.

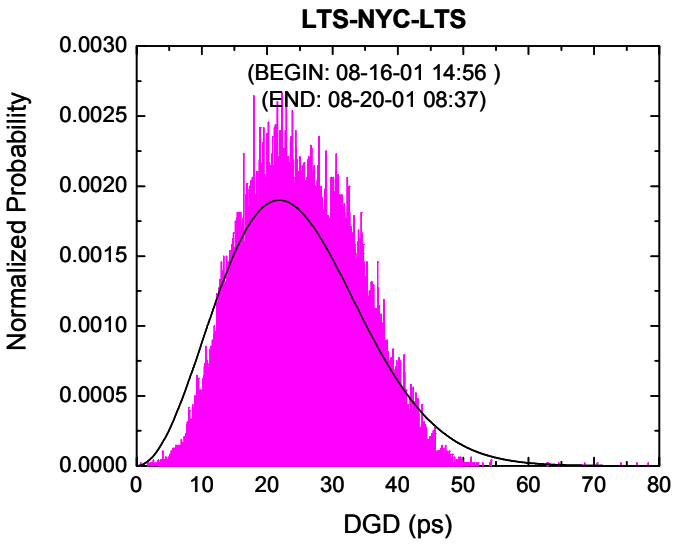

Figure 17. Measured DGD on ATDNET to BossNet connection.

In Figure 18 the PDL distribution on BossNet is shown. Note the mean PDL is near 2 dB but that the PDL can exceed 4 dB which can cause significant signal-to-noise degradation [4].

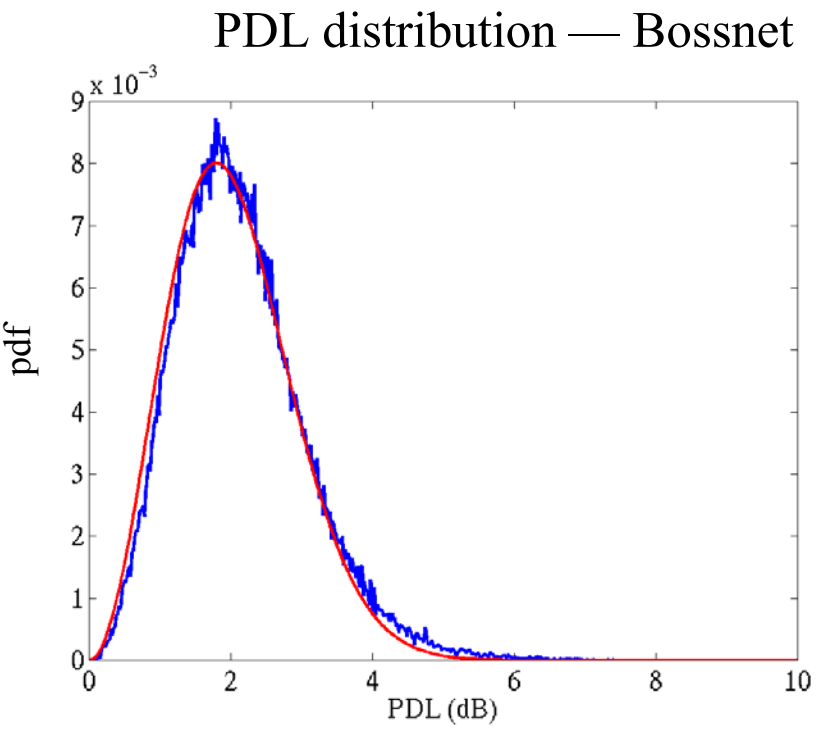

Figure 18. PDL distribution on BossNet.

New fiber has been installed on ATDNET which has significantly smaller DGD. The mean values of DGD are less than 1 ps over typical links in the network. Ongoing experiments in follow-on studies of this research are examining the statistics of this new fiber. It appears that these levels are small enough to permit 40 Gb/s data transmission.

The polarization studies presented in this report have significant implications for all-optical networks. As in the case of dispersion, the variability of the PMD and PDL is the key issue. If one network is optically connected to another such as ATDNET and BossNet, the performance of the entire transmission may be hampered by the segment of the network with the largest DGD and PDL. This is not a static problem that can be programmed into network management software since the DGD and PDL in any segment can vary over time. The time variation is not easy to model and at the moment real network performance appears much more complicated than the simple models that have been presented. This variability will likely be an issue for many years since installed fiber is expensive to replace. Thus it is likely that many

networks will continue to contain segments that have large values of PMD. This may limit the ability of these networks to upgrade to higher data rates.

IV. Conclusions

This research demonstrated the ability to transmit data at low error rates on installed optically switched metropolitan and long-haul networks at 10 Gb/s. This is significant since transmission across networks with very different designs and fiber plants was successful. At data rates of 10 Gb/s, degradation was observed due to nonlinear interactions in the optical fiber even over transmission distances as short as 400 km. These effects could be partially mitigated by using the correct dispersion distribution in the network. This implies that the network management process will have to be able to alter the dispersion profile at the transmitter and receiver as the transmission route is altered. Data rates of 20 Gb/s per second were successful on the metropolitan network, but errors increased on the long-haul network due to signal-to-noise degradation. This implies future high speed experiments on these interconnected networks will have to use lower loss connections.

At 40 Gb/s even the transmission experiments on ATDNET failed due to large values of PMD. The PMD statistics were found to vary from segment to segment over the network. Further, the PMD varied in each segment as a function of time. There is some evidence that the variations are not random and may be due to forcing functions like wind. It is clear that existing models of PMD may not be adequate for predicting performance in real networks.

New fiber installed on ATDNET shows promise of achieving 40 Gb/s transmission due to low levels of PMD.

V. References

1. “Experimental and Theoretical Characterization of a 40-Gb/s Long-Haul Single-Channel Transmission System”, Ronald Holzlöhner ; Heider N. Ereifej ; Vladimir S. Grigoryan ; Gary M. Carter ; Curtis R. Menyuk, IEEE Journal of Lightwave Technology Vol. 20 pp. 1124-1131(2002).

2. “Quantitative Experimental Study of Intra-Channel Nonlinear Timing Jitter in a 10 Gb/s Terrestrial WDM Return-to-Zero System,” H. Xu, H. Jiao, J. Wen, J. Zweck, L. Yan, C. Menyuk, G. Carter, University of Maryland Baltimore County, Baltimore, MD; G. Carter, paper to be presented at OFC 03, March 23-28, 2003, Atlanta, GA.

3. “Polarization Mode Dispersion”, Herwig Kogelnik, Rober M. Jopson, and Lynn E. Nelson, Optical Fiber Telecommunications IV B, Ivan Kaminow and Tingye Li eds, Academic Press, San Diego (2002) Chapter 15.

4. “The Need for Dynamic Control in High Data-Rate Communication Systems”, Gary M. Carter, Presentation at Summer Topical Meeting on Dynamic Enablers of Next-Generation Optical Communication Systems, Mont Tremblant, QC Canada 15-17 July 2002 sponsored by IEEE LEOS.

Note: References 1, 2 and 3 above are reproduced in Appendix A.

APPENDIX A: PUBLISHED PAPERS

Experimental and Theoretical Characterization of a 40-Gb/s Long-Haul Single-Channel Transmission System

Ronald Holzlöhner, *Student Member, IEEE*, Heider N. Ereifej, *Member, IEEE*, Vladimir S. Grigoryan, *Member, IEEE*, Gary M. Carter, *Member, IEEE*, and Curtis R. Menyuk, *Fellow, IEEE*

***Abstract*—We present a comparison between experiment and simulation of a 40-Gb/s periodically stationary dispersion-managed soliton (DMS) system in a recirculating loop. We find that we can propagate an error-free signal over 6400 km at 40 Gb/s and over 12 000 km if we lower the data rate to 10 Gb/s, keeping all other parameters constant. A careful analysis of the limiting factors shows the strong influence of nonlinear optical pulse-to-pulse interactions, causing a large increase in timing jitter. At a transmission distance of 6400 km, a large fraction of the jitter is due to pulse-to-pulse interactions. Moreover, we find that the system performance is very sensitive to parameter variations. We conclude that periodically stationary DMS systems suffer from numerous problems when increasing the data rate, suggesting that it may be impractical for wavelength-division multiplex transmission at 40 Gb/s.**

***Index Terms*—Amplified spontaneous emission noise, dispersion management, modeling, optical fiber transmission, optical solitons, timing jitter, transmission-line theory.**

I. Introduction

EXTENDING data rates in current optical transmission systems from 10 to 40 Gb/s promises large advantages but also poses great challenges. The sensitivity of the performance to variations in the system parameters is much larger at 40 Gb/s than at 10 Gb/s. There are many complications that appear when increasing the data rate, and careful experimental verification is needed after the system design stage. While there are a number of papers on 40-Gb/s periodically stationary dispersion-managed soliton (DMS) systems [1]–[3], there are few investigations of the underlying physics that limits the transmission distance. In this paper, we compare theory and experiment in a 40-Gb/s recirculating loop of length 107 km. We discuss the optimization of the map design and investigate the system performance as we vary operating parameters such as the optical power, erbium-doped fiber amplifier (EDFA) location, filter bandwidth, and central wavelength. We emphasize that this system does not operate in the quasi-linear DMS regime [4] but at a peak power of about 8 mW, which makes the transmission significantly nonlinear. Moreover, the pulses are approximately periodic with respect to the dispersion map. However, we anticipate some of the results of this work to be relevant to a wider class of systems.

The key detrimental effects that limit the achievable transmission distance in most optical systems are amplitude and timing jitter. Our results show that in our test system, the timing jitter is larger at 40 Gb/s than at 10 Gb/s due to nonlinear optical pulse-to-pulse interactions [5]. This result is significant, since error-free detection is limited to about 5.5 ps of timing jitter in a 10-Gb/s system and to about 1.5 ps at 40 Gb/s [6]. By contrast, we observe that the fluctuation in the pulse energy is about the same at 40 and 10 Gb/s. To make a meaningful comparison and to isolate the impact of pulse-to-pulse interactions on the signal evolution, we prepared our test system to operate in two different modes. In the first mode, we transmitted pseudorandom bit sequences at 40 Gb/s that have a ratio of marks to spaces of 1 : 1, and we will refer to this mode as the 40-Gb/s mode of operation. The second mode is identical to the first, except that the bit pattern was changed to a marks-to-spaces ratio of 1 : 4. There were at least two spaces between each two marks, thereby eliminating pulse-to-pulse interactions. Consequently, the second mode corresponds to transmission at 10 Gb/s while operating with the same pulse parameters, in particular, the same pulse duration and peak power, as the first mode. We will refer to the second mode as the 10_{40} Gb/s mode of operation and stress that it differs from an optimized 10-Gb/s transmission that would use longer pulses and possibly different peak powers.

Measuring and simulating optical timing jitter in a 40-Gb/s system with a precision of under 1 ps is challenging, and the result depends on the exact definition of timing jitter. This paper is one of the first that addresses this complex issue and compares results obtained from different methods in the context of a 40-Gb/s system. We present a detailed study of the jitter evolution and the sources of error in its measurement. In particular, we review the measurement of amplitude and timing jitter using an eye diagram, and, at 10 Gb/s, a method introduced by Mollenauer [7] that relies on the fading of radio-frequency (RF) tones with transmission distance. We then compare the results with the common theoretical definition of timing jitter as a variation in the central pulse time [8]. We show that optical

Manuscript received December 17, 2001. This work was supported in part by the National Science Foundation and in part by the U.S. Department of Energy.

R. Holzlöhner and V. S. Grigoryan are with the Department of Computer Science and Electrical Engineering, University of Maryland Baltimore County, Baltimore, MD 21250 USA (e-mail: holzloehner@umbc.edu).

H. N. Ereifej is with the Laboratory for Physical Sciences, College Park, MD 20740 USA.

G. M. Carter is with the Department of Computer Science and Electrical Engineering, University of Maryland Baltimore County, Baltimore, MD 21250 USA and the Laboratory for Physical Sciences, College Park, MD 20740 USA.

C. R. Menyuk is with the Department of Computer Science and Electrical Engineering, University of Maryland Baltimore County, Baltimore, MD 21250 USA and PhotonEx Corporation, Maynard, MA 01754 USA.

Publisher Item Identifier 10.1109/JLT.2002.800343.

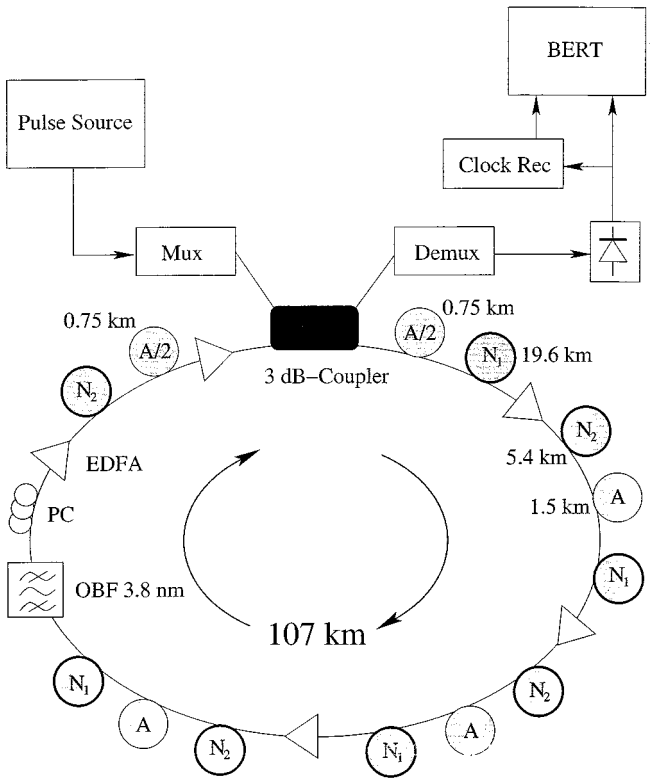

Fig. 1. Simplified experimental setup. The labels A, N_1, and N_2 denote fiber spans of anomalous and normal dispersion, respectively. PC denotes the polarization controller, OBF the inline optical bandpass filter, Clock Rec the clock recovery circuit, and BERT the bit-error-rate tester.

pulse-to-pulse interactions limits the maximum error-free transmission distance at 40 Gb/s to 6400 km. However, our simulations indicate that reducing the length of the dispersion map by 15% would extend the transmission distance to 10 000 km by minimizing the pulse-to-pulse interactions.

The remainder of this paper is organized as follows: In Section II, we describe the experimental setup and the numerical simulation techniques. In Section III, we compare definitions of amplitude and timing jitter and their measurement, discuss dispersion map optimization, and compare the results of experiment and simulation. Section IV contains the conclusions.

II. Experimental Setup and Theory

A. Experimental Setup

We evaluated the transmission performance of our test system both experimentally and through computer simulations. Fig. 1 shows a sketch of the recirculating loop experiment. A mode-locked fiber laser manufactured by PriTel generated the pulses of 4.5-ps full-width half-maximum (FWHM) pulse duration with a repetition rate of 10 GHz. The data stream was modulated at 10 Gb/s with a $2^{23}-1$ pseudorandom bit sequence using a $LiNbO_3$ intensity modulator. The signal was then multiplexed using a two-stage optical time-division multiplexer (TDM), the first one multiplexing the signal up to 20 Gb/s and the second one to 40 Gb/s, by interleaving the 10-Gb/s data stream with a copy of itself that was delayed by about 1 ns. The signal remained unchirped and passed a 3-dB coupler that inserted it into the loop with a peak power of 7.6 mW. All pulses were copolarized. The pulses had a Gaussian shape, and their duration assumed an equilibrium value of $\tau_{\rm opt} = 6$ ps in the loop, measured at the launch point in the map after a few round trips. The average optical power was 1.5 dBm at 40 Gb/s and -3.5 dBm at 10_{40} Gb/s.[1] The center of the launch pulse spectrum lay at 1551.5 nm, while the center of the filter transmission curve was slightly shifted to $\lambda_F = 1551.6$ nm. The offset seemed to help somewhat in shaping the equilibrium pulse but was small compared to the optical bandwidth of about 0.61 nm. The recirculating loop contained four dispersion map periods with a combined length of 106.7 km. Each period of the dispersion map consisted of a 25-km span of normal fiber with dispersion of -1.02 ps/nm-km followed by a 1.5-km span of anomalous fiber with dispersion of 17 ps/nm-km. The path average dispersion was in the range 0.005–0.025 ps/nm-km, depending on λ_F, and the dispersion slope was $dD/d\lambda = 0.0768$ ps/nm^2-km, where D is the local dispersion. Each map period contained an EDFA that divided the normal span into pieces of length 19.6 and 5.4 km, respectively, and we denote the corresponding fiber spans in Fig. 1 by N_1 and N_2. This location minimizes pulse stretching and hence pulse-to-pulse overlap, as we will discuss in Section III-B. The fourth map contained a 3.8-nm optical bandpass filter to reduce the noise, and its anomalous span was split in half by inserting a fifth EDFA, an acoustooptical (AO) loop switch, and the 3-dB coupler in the middle of the span. This map design is based on the 10-Gb/s system described in [9], with the dispersion map length divided by a factor of four. The optical TDM demultiplexer consisted of two stages: an electrooptic $LiNbO_3$ modulator manufactured by Sumitomo that demultiplexed from 40 to 20 Gb/s, and an electroabsorption modulator (JAE) that demultiplexed from 20 to 10 Gb/s.

B. Modeling Setup

We use the scalar split-step method to simulate the light propagation in a time window of 3.2 ns, containing 128 bits at 40 Gb/s and 32 bits at 10 Gb/s. In the recirculating loop that we are modeling, the polarization-dependent loss is about 0.35 dB per round trip and the polarization controllers are optimized to pass the signal with minimum loss, yielding a polarization degree of $>$95%. Consequently, the polarization orthogonal to the signal is suppressed. In the simulations, as in the experiment, we assume copolarized pulses. We run Monte Carlo simulations in which a different bit sequence is chosen for each realization; the ratio of marks to spaces is always 1 : 1. The EDFAs are modeled as saturable amplifiers with a saturation time of 1 ms and a saturation power of 10 mW. Details on the simulation procedure can be found in [9]. The spontaneous emission factor is $n_{\rm sp} = 1.2$. At the receiver, we include the optical TDM demultiplexer, the clock recovery circuit, and the 20-Gb/s bandwidth-limited photodiode in the simulation model. We note that proper receiver modeling becomes more critical as we go from 10 to 40 Gb/s. For

[1]In order to maintain equal pulse peak powers, we would have had to reduce the average power at 10_{40} Gb/s to $1.5 - 6 = -4.5$ dBm. However, we were not able to lower the EDFA gains that much without increasing $n_{\rm sp}$.

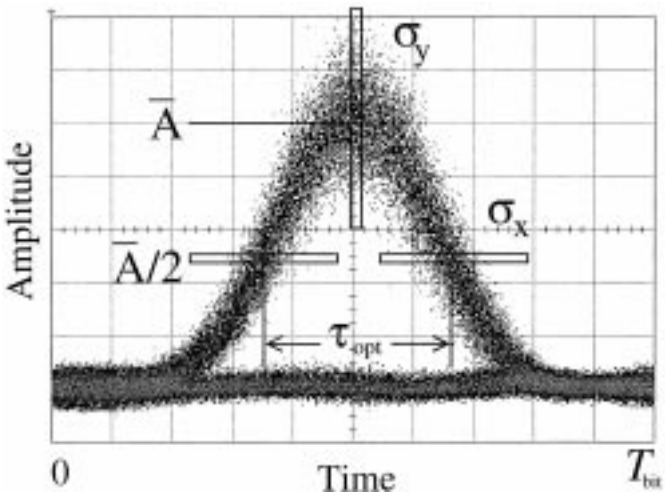

Fig. 2. Schematic of amplitude and timing jitter measurement using a digital oscilloscope. The vertical box is used to measure the absolute amplitude jitter σ_A, and the horizontal boxes are used to measure the absolute timing jitter σ_{t_0}.

example, our 20-GHz photodiode, followed by amplifiers and cables, broadens the received pulses from 6 ps to 23–30 ps, and hence the impulse response of the receiver system has a major influence on the eye diagram. This broadening was not as important in previous 10-Gb/s experiments [9]. We model the effective demultiplexer window function using a Butterworth function $f(t) = 1/[1 + |2(t - t_0)/T_{\mathrm{FWHM}}|^k]$, where t is time, t_0 is the central time of the window, $T_{\mathrm{FWHM}} = 26$ ps is the window duration, and $k = 6.5$ (note that the demultiplexer is not a Butterworth filter, but rather the window function in time happens to follow the Butterworth function). This fitting function is in good agreement with the experimentally measured demultiplexer shape.

III. Results and Discussion

A. Amplitude and Timing Jitter

We find that the values of amplitude and timing jitter depend strongly on the measurement method and that their accurate determination is challenging, in both simulation and experiment. In this section, we will outline the problems we encountered and discuss their solutions.

It is common practice to measure amplitude and timing jitter using the eye diagram on a digital sampling oscilloscope, as shown schematically in Fig. 2. A large number of samples is accumulated in the elongated vertical and horizontal boxes, and the sample histogram as a function of the positions along the long side of the boxes is produced. We denote the mean of the data in the vertical box, which is the mean amplitude, by $\overline{A}$, and the standard deviation of its sample points by σ_y. The difference of the means of the horizontal boxes at amplitude $\overline{A}/2$ is the mean FWHM electrical pulse duration τ, and the symbols $\sigma_{x,l}$ and $\sigma_{x,r}$ denote the standard deviations of the data in the left and right boxes, respectively. Then we define $\sigma_x^2 = (\sigma_{x,l}^2 + \sigma_{x,r}^2)/2$. We call this method of determining the amplitude and timing jitter the scope method.

With the optical field envelope $u(t)$, where t is time, we define the quantities

$$U = \int_0^{T_{\mathrm{bit}}} |u|^2 \, dt \tag{1a}$$

$$t_0 = \frac{1}{U} \int_0^{T_{\mathrm{bit}}} t|u|^2 \, dt \tag{1b}$$

where T_{bit} is the bit duration, U is the pulse energy, and t_0 is the central time of the pulse. If we assume that the pulses after optical filtering and bandwidth-limited square-law detection are Gaussian, so that $|u(t)|^2 = A\exp[-t^2/(2s^2)]$ with an electrical FWHM pulse duration $\tau = 2s\sqrt{2\ln 2}$, then the amplitude is $A = (2U/\tau)\sqrt{\ln 2/\pi}$. We stress again that A depends on τ, and in our system τ is in the range of 23–30 ps, owing to the bandwidth-limited receiver, while the pulse duration in the optical fiber is only $\tau_{\mathrm{opt}} = 6$ ps. This bandwidth limitation makes A a more robust quantity with regard to high-frequency amplified spontaneous emission (ASE) noise that is irrelevant to the detector.

The eye diagram of a signal with finite timing jitter and zero amplitude jitter can have nonzero σ_y; and conversely a signal with finite amplitude jitter and zero timing jitter will yield a nonzero σ_x. In other words, σ_x and σ_y depend in a complicated way on σ_{t_0} and σ_A, the standard deviations of t_0 and A, respectively. We define a dimensionless timing jitter $\Sigma_{t_0} = \sigma_{t_0}/\tau$ [8], where τ is the average FWHM pulse duration. Analogously, we define the dimensionless energy jitter $\Sigma_A = \sigma_A/\overline{A}$, where $\overline{A}$ is the average of the pulse amplitudes A. A first-order approximation, under the assumptions that amplitude and timing fluctuations are statistically independent and τ is constant, is

$$\frac{\Sigma_x}{\Sigma_{t_0}} \approx \sqrt{1 + \left(0.361\frac{\Sigma_A}{\Sigma_{t_0}}\right)^2} \tag{2}$$

where $\Sigma_x = \sigma_x/\tau$. Large ratios of amplitude jitter to timing jitter hence lead to sizable deviations between Σ_x and the relative timing jitter Σ_{t_0}. In our simulations at 10_{40} Gb/s, we obtain after 8400 km the values $\Sigma_A = 7.2\%$, $\sigma_{t_0} = 1.16$ ps, and $\tau = 23$ ps, yielding $\Sigma_x/\Sigma_{t_0} = 1.12$. This jitter enhancement can be even more deceptive when the amount of amplitude jitter in experiments is underestimated due to the common use of deeply saturated electrical amplifiers in the receiver, as discussed in the next section. In (2), the assumption of a constant τ seems to be very strong, and in reality τ fluctuates. However, our experimental timing jitter results are in good agreement with (2), and the approximation serves to show the need for an exact definition of amplitude and timing jitter.

To verify the timing jitter results, we employed a second measurement method that was introduced by Mollenauer and is based on the fading of the RF tones over propagation distance [7]. Due to timing jitter, energy diffuses from the frequency mode at $1/T_{\mathrm{bit}}$ and its harmonics to neighboring frequencies. We expect the normalized timing jitter obtained from this method to be closer to Σ_{t_0} than to Σ_x, and we will show a comparison in the next section.

Amplitude and timing jitter are also enhanced by the optical TDM demultiplexer, whose window function is not square

and thus causes power to leak into adjacent bit slots at the receiver. Even in the absence of pulse leakage, the curvature of the window near the top increases amplitude jitter by attenuating pulses that lie off-center relative to the window.

B. Map Optimization

In this section, we show that the admissible parameter range for transmission of DMS pulses at 40 Gb/s is much smaller than at 10 Gb/s in periodically stationary DMS systems and discuss some of the tradeoffs involved in the parameter optimization.

We consider the dispersion map strength $\gamma = [(\beta_n'' - \beta_{\rm ave}'')L_n - (\beta_a'' - \beta_{\rm ave}'')L_a]/\tau_{\rm opt}^2$, where β_a'', β_n'' and L_a, L_n represent the dispersion values and lengths of the anomalous and normal spans, respectively, $\beta_{\rm ave}'' = (\beta_a'' L_a + \beta_n'' L_n)/(L_a + L_n) = -D_{\rm ave}\lambda_F^2/2\pi c$ is the path average dispersion, and $\tau_{\rm opt}$ is the minimum FWHM pulse duration in the dispersion map [10]. All dispersion values are taken at the central filter wavelength λ_F. In our system, the map strength is $\gamma = 1.95$, corresponding to an energy enhancement of 3.4 and a maximum pulse duration of about 12 ps. As noted in [1], there is a tradeoff in choosing the optimum map strength. Large map strengths and hence stretching factors tend to reduce the Gordon–Haus jitter by a factor on the order of the square root of the enhancement factor [11], [12]. However, if the pulse durations become too large, the pulse tails overlap and start interacting nonlinearly, giving rise to pattern-dependent signal distortion [13], [14], as well as to shifts in the central times of the pulses [15]. The development of ghost pulses that was described in [13] is small in our system at the error-free transmission distances. In our setup, the map strength is slightly larger than optimal, and the nonlinear pulse-to-pulse interactions are our main limiting factor at 40 Gb/s. Earlier work showed that the pulse-to-pulse interactions in a DMS system can be minimized by reducing γ to 1.66 for a value of $T_{\rm bit} \approx 4\tau_{\rm opt}$, where $T_{\rm bit} = 25$ ps is the bit window, equaling the minimum pulse spacing [15]. Our simulations show that by scaling all fiber span lengths by $1.66/1.95 = 0.85$, leading to a dispersion map period of 90 km and an amplifier spacing of 22.6 km, pulse interactions at 40 Gb/s can be removed almost completely and error-free transmission over 10 000 km becomes possible.

In a system with significant nonlinearities, the maximum pulse duration of the pulses in the dispersion map is not determined by the value of γ alone but also strongly depends on the location of the EDFAs in the dispersion map [16]. Fig. 3 shows the evolution of the FWHM pulse duration for one round trip in the recirculating loop. The distance is scaled by the magnitude of the local dispersion so that the anomalous (A) and normal (N) fiber spans appear to have equal lengths. The three curves correspond to placing the EDFAs 0, 5, and 20 km after the beginning of the normal dispersion span, respectively. The corresponding maximum pulse durations are 14.3, 12.5, and 11.6 ps, respectively, at the ends of the normal spans. Our simulations show that the maximum pulse duration is globally minimized when the first four EDFAs are placed at 20 km from the beginnings of the normal dispersion spans. Also, the overall timing jitter at 40 Gb/s is minimized in this case. In the simulations, we also tried to launch the signal at different points in the anomalous span, equivalent to prechirping the pulses. However, we found that launching in the middle of the anomalous span, as was done in the experiments, was optimal.

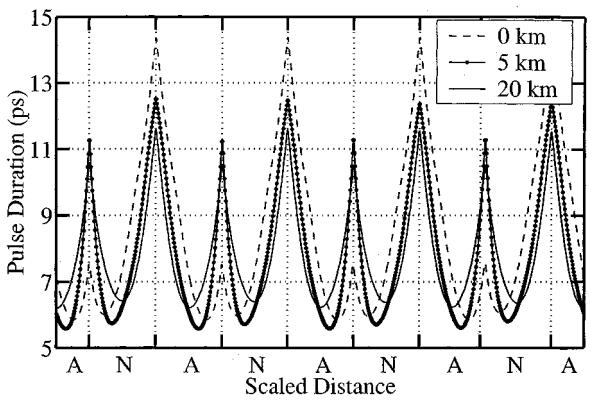

Fig. 3. Evolution of the FWHM pulse duration during one round trip in the recirculating loop for three different EDFA locations in the normal dispersion span. The distance is scaled by the magnitude of the local dispersion so that the anomalous (A) and normal (N) fiber spans appear to have equal lengths.

In the simulations, we observe that neighboring pulses attract each other and tend to reduce their separation in time as they propagate, regardless of their initial phase difference. The pulse-to-pulse attraction is only reduced by 5% when we alternate the phases of adjacent pulses by π, compared to constant phase. This result is consistent with Yu *et al.* [15], who find that the timing jitter is independent of the optical phase when $\gamma \gtrsim 1.65$. (Note that our definition of γ differs from that of Yu *et al.* by a factor of 2.) The physical reason lies in the rapid phase changes due to strong dispersion management. In noise-free simulations of our system, on the other hand, alternating the phase reduces the mutual pulse attraction by as much as 50%, indicating that launching a noise-free phase-alternating signal leads to a mathematically unstable minimum in the pulse attraction.

A tradeoff that is more critical at 40 Gb/s than at 10 Gb/s is the choice of the path average dispersion $D_{\rm ave}$. Larger values of $D_{\rm ave}$ keep the entire pulse spectral range in the anomalous dispersion regime, which tends to stabilize the soliton pulse shapes. On the other hand, the timing jitter grows with $D_{\rm ave}$. Although we can achieve an optimum transmission distance of 18 000 km at 10_{40} Gb/s with $D_{\rm ave} \approx 0.03$ ps/nm-km, this dispersion value is too large at 40 Gb/s due to the increased sensitivity to timing jitter. A similar tradeoff applies to the optimum optical peak power. On one hand, a higher peak power improves the optical signal-to-noise ratio, but on the other hand, it enhances nonlinear pulse-to-pulse interactions.

C. Comparison of Simulation and Experiment

In the experiment, we optimized the loop parameters to achieve the maximum transmission distance at 40 Gb/s. To isolate the impact of nonlinear pulse-to-pulse interactions, we then compared the 40-Gb/s system to a system at the reduced data rate of 10 Gb/s while keeping all other parameters constant, denoted by 10_{40} Gb/s. In particular, we still used the optical TDM demultiplexer at 10_{40} Gb/s. Therefore, our 10_{40} Gb/s transmission was almost identical to the 40-Gb/s case, except that the minimum pulse spacing was 100 ps.

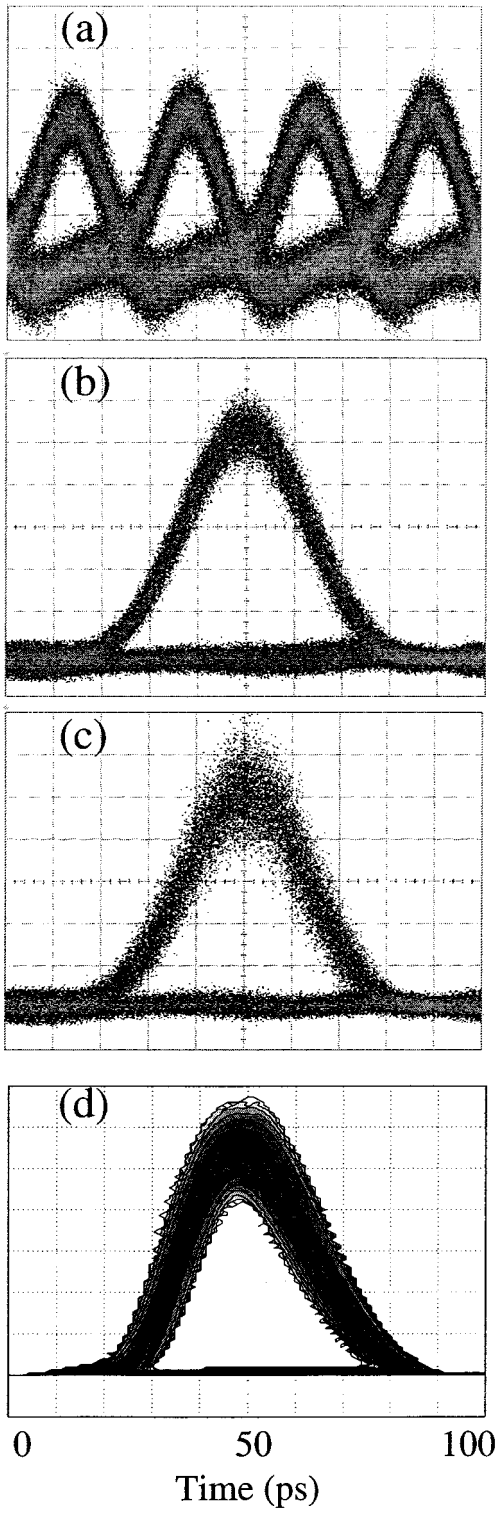

Fig. 4. (a) Input pulse train at 40 Gb/s, measured with a 40-GHz photodiode. (b) Eye diagram of a pulse after 0 km (back-to-back) at 40 Gb/s measured at the output of a 20-GHz photodiode. (c) Eye diagram of a pulse after 6000-km propagation. (d) Contour plot of probability densities of the simulated photodiode current.

Fig. 4 shows the eye diagram at 40 Gb/s without using electrical narrow-band filters. Fig. 4(a) shows the 40-Gb/s pulse train before it is inserted into the loop, using a 40-Gb/s monitor photodiode. This photodiode has a high electrical bandwidth,

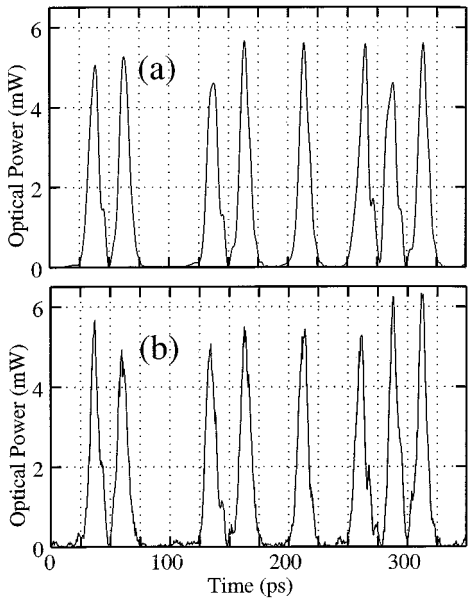

Fig. 5. Optical power at 40 Gb/s after 6400 km at the maximum expansion point in the map. Simulation (a) without ASE noise and (b) with noise. The noise-free signal in (a) shows a strong pulse distortion that is entirely due to pulse-to-pulse interactions.

but it also produces a large amount of electrical noise. Therefore, we did not use it to measure eye diagrams. Fig. 4(b) and (c) shows the eye diagrams of a single pulse in the demultiplexed signal at 0 km and 6400 km, respectively, using a 20-Gb/s photodiode. No electrical filtering was applied to the signal. Fig. 4(d) shows the simulated eye diagram in the form of a contour plot. The slightly asymmetrical pulse shape is due to the electrical modeling of the bandwidth-limited photodiode.

Fig. 5 shows the optical power in the 40-Gb/s simulations after 6400 km. The data were extracted after the normal fiber span, where pulses are maximally expanded, corresponding to the location of the four largest peaks in Fig. 3. Comparing Fig. 5(a), where the ASE noise was turned off in all the EDFAs, with Fig. 5(b) being with the noise turned on, we observe that a large part of the pulse distortion is present in the absence of noise. Isolated pulses, such as the fifth pulse in (a), all evolve identically when the ASE noise input is turned off; hence, this distortion must be due to pulse-to-pulse interactions. The peak power fluctuation in (a) is mostly due to the significant pulse shape distortion and does not imply a large pulse energy fluctuation Σ_A. Instead, Σ_A is mostly caused by noise and is about six times larger in (b) than in (a). Note also that the noise in the zeros in (b) is small.

Fig. 6 shows the timing jitter evolution at 40 Gb/s and at 10_{40} Gb/s for both experiment and simulation using the scope method, where the crosses and circles show the experimental and the curves show the numerical results. In the simulations, we emulate the statistical function of the digital oscilloscope described in Section III-A using Monte Carlo simulations, rather than using the central time definition of the timing jitter. The initial jitter of about 0.2 ps is due to our suboptimal demultiplexing, leading to the leakage of neighboring pulses into the demultiplexer window. Error-free data transmission breaks down after 6400 km at 40 Gb/s and after 12 000 km at 10_{40} Gb/s.

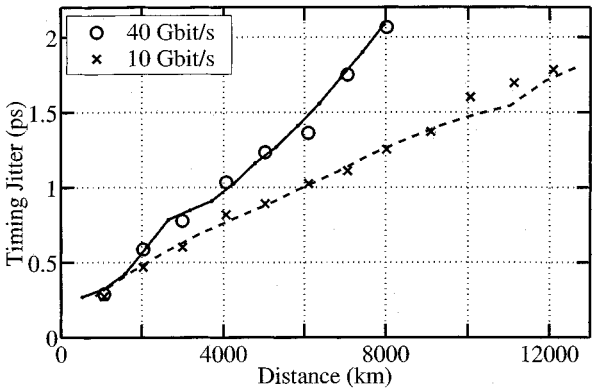

Fig. 6. Timing jitter at 40 and 10_{40} Gb/s using the scope method. The circles and crosses show the experimental measurement, and the lines show the simulation results.

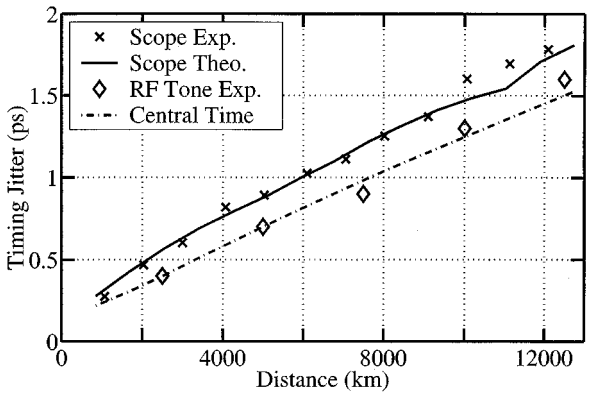

Fig. 8. Comparison of the scope method and the RF tone fading method at 10_{40} Gb/s to highlight jitter enhancement.

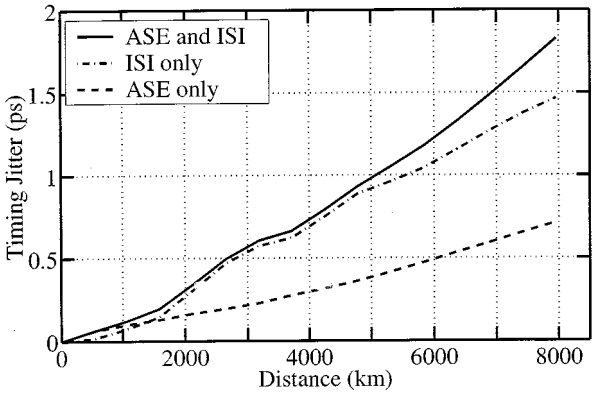

Fig. 7. Timing jitter contributions in the 40-Gb/s simulation with a perfect (square) demultiplexer window. All curves show timing jitter according to the central time definition. Solid line: full simulation. Dash-dotted line: no ASE noise ($n_{\rm sp} = 0$), exhibiting pulse-to-pulse interactions only. Dashed line: timing jitter with ASE noise, but with the bit pattern $101010\cdots$ instead of a random bit pattern, therefore removing pulse-to-pulse interactions.

The reduced timing jitter at 10_{40} Gb/s is due to the absence of pulse-to-pulse interactions. Note that $n_{\rm sp}$ is slightly larger at 10_{40} Gb/s than at 40 Gb/s; the two curves would diverge even further with equal values of $n_{\rm sp}$. The breakdown of the transmission occurs in two stages: a first stage at 6400–7500 km, in which the error rate exceeds 10^{-9} mainly due to timing jitter; and a second stage beyond 7500 km, where the pulses themselves break down due to pulse-to-pulse distortion and ASE noise. The present system is limited by timing jitter, not by noise in the zeros, as was the case in earlier 10-Gb/s experiments [9]. As a consequence, the bandwidth and exact filter profile of the optical inline filter are of less importance. We varied filter types and the filter bandwidth between 2.8 and 4.6 nm without observing large differences in the maximum transmission distance. If we were able to extend the transmission at 40 Gb/s to distances beyond 12 000 km, our previous modeling [16] shows that DMS robustness would critically depend on the optimization of the inline filter.

Fig. 7 compares the evolution of the jitter of the central time Σ_{t_0} in the simulations for three different cases; we used an ideal (square) demultiplexer window to eliminate eye degradation due to the demultiplexer. The solid curve shows the timing jitter resulting from the full simulations, including ASE noise, at 40 Gb/s. The dash-dotted line shows the same timing jitter in the absence of ASE noise, exhibiting the effect of pulse-to-pulse interactions only. The dashed line is the timing jitter with ASE noise, but with the alternating bit pattern $101010\ldots$ instead of a random bit pattern, thereby removing the pulse-to-pulse interactions. The latter procedure allows a more accurate isolation of pulse-to-pulse effects than reducing the data rate to 10_{40} Gb/s, since the average power in the loop is kept strictly constant in the presence of saturable EDFAs. Again, one can see the significant impact of pulse-to-pulse interactions on the timing jitter. However, the fact that the curves for the noisy and noise-free signals are so close does not mean that noise is negligible in this system. Weak noise breaks the unrealistic perfect phase symmetry between adjacent pulses and might mitigate their mutual attraction in the beginning, while at larger distances increasing the timing jitter. According to [13] and [17], pulse-to-pulse attraction due to intrachannel cross-phase modulation (XPM) depends on the ratio $x = \tau_{\rm opt}/T_{\rm bit}$, where $\tau_{\rm opt}$ is the optical FWHM pulse duration and $T_{\rm bit}$ is the bit duration. The magnitude of the attraction is proportional to $\exp(-1/2x^2)/x^3$. This function has an extremely steep slope for $0.3 < x < 1$. The maximum value that x assumes during the first loop revolution is $x = \tau_{\rm opt}/T_{\rm bit} = 12$ ps/25 ps $= 0.48$, resulting in a pulse-to-pulse attraction of 8.7% relative to its maximum near $x = 1$. This attraction is only effective over the short range in the map where the pulse duration is close to its maximum; see Fig. 3. However, once the pulses approach each other, the effective $T_{\rm bit}$ is reduced, the ratio x increases, and hence the attraction grows very fast.

In Fig. 8, we show the timing jitter σ_x measured by the scope using crosses and the results of the RF tone measurement using diamonds. Since the bandwidth of our electrical equipment is limited to about 40 Gb/s, we can only apply the RF tone method to 10_{40} Gb/s transmission [5]. The solid line represents the simulation result of the absolute timing jitter from the scope method σ_x, while the dashed line shows the simulation result of σ_{t_0} (central time method). The difference between the curves amounts to 10–20%, depending on the amplitude jitter at each data point, and agrees with (2). On the other hand, note the good agreement between the RF tone method and σ_{t_0}.

Fig. 9 exhibits the squared normalized energy variance Σ_A^2 in the 40 Gb/s and 10_{40} Gb/s simulations. The dashed line is a

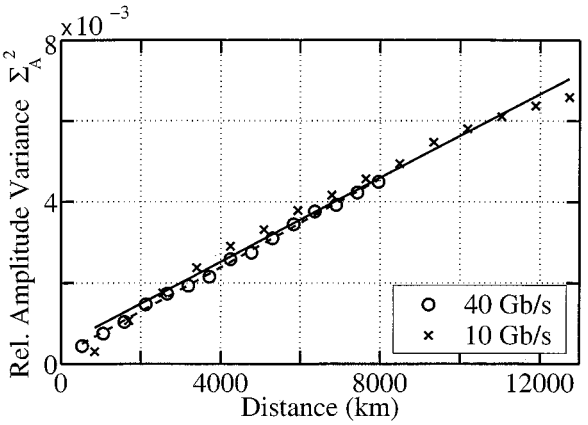

Fig. 9. Relative energy variance, Σ_A^2, in the 40- and 10_{40}-Gb/s simulations. The dashed line is a linear fit to the measured results at 40 Gb/s, and the lines are fits to the 10_{40}-Gb/s results.

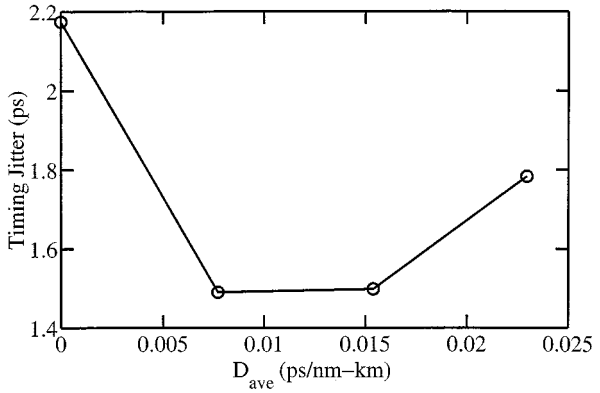

Fig. 10. Dependence of the timing jitter on the path-average dispersion D_{ave} at 40 Gb/s after 6400 km. The wavelength is increased by 0.1 nm for each data point.

linear fit to the measured results at 40 Gb/s and the solid line to the 10_{40}-Gb/s results. The values at 40 Gb/s and 10_{40} Gb/s are almost identical, indicating that little energy is transferred between pulses when they interact nonlinearly, and the energy jitter is mainly due to ASE noise energy that grows linearly with distance [8]. We found that the impact of energy jitter can easily be underestimated due to the use of saturated electrical amplifiers. Our Anritsu RF amplifier, located between the photodiode and the bit error rate tester (BERT), is deeply saturated and hence compresses the rail of the ones in the eye diagram compared to the zeros rail. Electrical amplifier saturation, in contrast to EDFA saturation, is a very fast process and hence distorts the signal shape. For this reason, we only used the RF amplifier to drive the BERT and not to produce any eye diagrams.

To highlight the sensitivity of the system to variations in the path-average dispersion, we simulated the signal propagation at different wavelengths. Fig. 10 shows the timing jitter as a function of D_{ave} at 6400 km. The data points correspond to a wavelength spacing of 0.1 nm, and the 40-Gb/s simulation was performed at $D_{\text{ave}} = 0.0154$ ps/nm-km. Although we have not attempted WDM transmission in the recirculating loop, it is obvious that the present third-order dispersion of $dD/d\lambda = 0.0768$ ps/nm^2-km is large enough to spread different channels over a large range of D_{ave}, resulting in increased timing

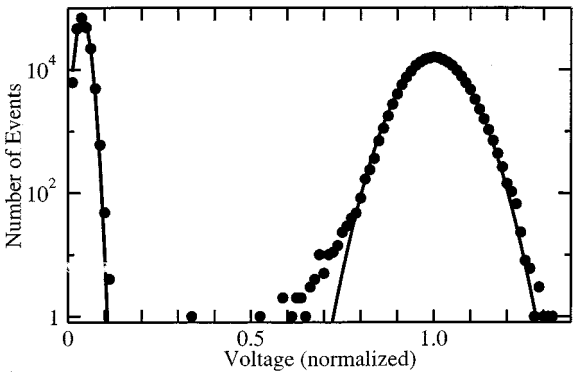

Fig. 11. Histogram of the narrow-band filtered receiver voltage at 40 Gb/s, resulting from the Monte Carlo simulation at a propagation distance of 7500 km. The left peak corresponds to the spaces, the right peak to the marks. The solid lines are Gaussian fits. The departure from the Gaussian behavior is obvious in the tails.

jitter in the edge channels. Our simulation shows that even in single-channel transmission, the third-order dispersion strongly deteriorates the signal and hence has to be taken into account, in contrast to previous 10-Gb/s systems with wider pulses [9]. The physical reason is that third-order dispersion leads to asymmetrical pulses; in the present 40-Gb/s system, the leading tails of the pulses are stretched out and interact with adjacent pulses.

Fig. 11 shows a histogram of the received voltage after narrow-band filtering at 40 Gb/s, obtained from the Monte Carlo simulation of 3000 realizations. The propagation distance is 7500 km, which is about 1200 km beyond the distance where error-free transmission breaks down. The solid lines are Gaussian fits to the data points, using their mean and variance. The Q-factor based on the Gaussian fits is still larger than six, indicating error-free transmission. However, due to the departure of the probability density from Gaussian shape, the true error rate exceeds 10^{-9}, as is the case in the experiment. We note that the distortion of the Gaussian distribution in Fig. 11 is so severe that even a fit to only the data points that are part of the low voltage tail of the distribution of the marks fails.

IV. Conclusions

We demonstrate good agreement between experiment and simulation of a 40-Gb/s periodically stationary dispersion-managed soliton system in a recirculating loop. We use periodic dispersion compensation and a 3.8-nm optical inline filter. Reducing the data rate to 10 Gb/s, while keeping all other parameters constant, we are able to isolate the impact of the nonlinear pulse-to-pulse interaction, and we find that it is the key limiting effect at 40 Gb/s. The simulation enables us to optimize path-average dispersion, optical power, and amplifier spacing within the normal dispersion fiber span, all of which have strong impact on the maximum transmission distance. Of lesser influence on the error-free transmission distance are the optical inline filter bandwidth, the precise pulse shape at the launch point for a given pulse duration, and a small initial wavelength offset between the launched signal spectrum and the transmission maximum of the optical inline bandpass filter. The simulation shows that our dispersion map strength of 1.95 is slightly larger than optimal and that error-free transmission

at 40 Gb/s can be extended to 10 000 km if we reduce the length of our map period by 15%. We emphasize that timing jitter and the pulse-to-pulse interactions are strongly coupled in our loop and limit the propagation distance. The accurate experimental determination of both the amplitude and the timing jitter is not simple, and we compare different definitions and measurement methods. In conclusion, we find that the system is very sensitive to changes in the system parameters and conclude that the periodically stationary DMS format may not be practical for WDM transmission at 40 Gb/s.

ACKNOWLEDGMENT

The authors thank J. Zweck and B. Marks for inspiring discussions and substantial help with the manuscript.

REFERENCES

[1] I. Morita, K. Tanaka, N. Edagawa, and M. Suzuki, "40 Gb/s single-channel soliton transmission over transoceanic distances by reducing Gordon–Haus timing jitter and soliton–soliton interaction," *J. Lightwave Technol.*, vol. 17, pp. 2506–2511, 1999.

[2] K. Suzuki, H. Kubota, A. Sahara, and M. Nakazawa, "40 Gbit/s single channel optical soliton transmission over 70 000 km using inline synchronous modulation and optical filtering," *Electron. Lett.*, vol. 34, pp. 98–100, 1998.

[3] G. Aubin, T. Montalant, J. Moulu, F. Pirio, J.-B. Thomine, and F. Devaux, "40 Gb/s OTDM soliton transmission over transoceanic distances," *Electron. Lett.*, vol. 32, pp. 2188–2189, 1996.

[4] F. Le Guen, S. Del Burgo, M. L. Moulinard, D. Grot, M. Henry, F. Favre, and T. Georges, "Narrow band 1.02 Tbit/s (51×20 Gbit/s) soliton DWDM transmission over 1000 km of standard fiber with 100 km amplifier spans," in *Proc. OFC'99*, Washington, DC, 1999, paper PD4.

[5] H. N. Ereifej, R. Holzlöhner, and G. M. Carter, "Inter-symbol interference and timing jitter measurements in a 40 Gb/s long-haul dispersion-managed soliton system," IEEE Photon. Technol. Lett., to be published.

[6] J. P. Gordon and H. A. Haus, "Random walk of coherently amplified solitons in optical fiber transmission," *Opt. Lett.*, vol. 11, pp. 665–667, 1986.

[7] L. F. Mollenauer, M. J. Neubelt, S. G. Evangelides, J. P. Gordon, and L. G. Cohen, "Experimental study of soliton transmission over more than 10 000 km in dispersion-shifted fiber," *Opt. Lett.*, vol. 15, pp. 1203–1205, 1990.

[8] V. S. Grigoryan, C. R. Menyuk, and R.-M. Mu, "Calculation of timing and amplitude jitter in dispersion-managed optical fiber communications using linearization," *J. Lightwave Technol.*, vol. 17, pp. 1347–1356, 1999.

[9] R.-M. Mu, V. S. Grigoryan, C. R. Menyuk, G. M. Carter, and J. M. Jacob, "Comparison of theory and experiment for dispersion-managed solitons in a recirculating fiber loop," *IEEE J. Select. Topics Quantum Electron.*, vol. 6, pp. 248–257, 2000.

[10] N. J. Smith, N. J. Doran, F. M. Knox, and W. Forysiak, "Energy-scaling characteristics of solitons in strongly dispersion-managed fibers," *Opt. Lett.*, vol. 21, pp. 1981–1983, 1996.

[11] N. J. Smith, N. J. Forysiak, and W. Doran, "Reduced Gordon–Haus jitter due to enhanced power solitons in strongly dispersion managed systems," *Electron. Lett.*, vol. 32, pp. 2085–2086, 1996.

[12] G. M. Carter, J. M. Jacob, C. R. Menyuk, E. A. Golovchenko, and A. N. Pillipetskii, "Timing-jitter reduction for a dispersion-managed soliton system: experimental evidence," *Opt. Lett.*, vol. 22, pp. 513–515, 1997.

[13] P. V. Mamyshev and N. A. Mamysheva, "Pulse-overlapped dispersion-managed data transmission and intrachannel four-wave mixing," *Opt. Lett.*, vol. 24, pp. 1454–1456, 1999.

[14] M. J. Ablowitz and T. Hirooka, "Resonant nonlinear intrachannel interactions in strongly dispersion-managed systems," *Opt. Lett.*, vol. 25, pp. 1750–1752, 2000.

[15] T. Yu, E. A. Golovchenko, A. N. Pilipetskii, and C. R. Menyuk, "Dispersion-managed soliton interactions in optical fibers," *Opt. Lett.*, vol. 22, pp. 793–795, 1997.

[16] V. S. Grigoryan, P. Sinha, C. R. Menyuk, G. M. Carter, and A. Hasegawa, "Long distance transmission of filtered dispersion-managed solitons at 40 Gb/s bit systems rate over 6400 km," in *1999 ROSC Symposium on Massive WDM and TDM Soliton Transmission*, A. Hasegawa, Ed. New York: Kluwer, 1999.

[17] J. Mårtensson, A. Berntson, M. Westlund, A. Danielsson, P. Johannisson, D. Anderson, and M. Lisak, "Timing jitter owing to intrachannel pulse interactions in dispersion-managed transmission systems," *Opt. Lett.*, vol. 26, pp. 55–57, 2001.

Ronald Holzlöhner (S'00) was born in Essen, Germany, on December 30, 1970. He received the M.S. degree in physics from the Technical University of Berlin, Germany, in 1998. He is currently pursuing the Ph.D. degree at the University of Maryland Baltimore County (UMBC).

He studied at the University of California, Santa Barbara, in 1995/1996 as a Fulbright Exchange Student. While at UMBC, he works part-time as a Consultant for Virtual Photonics, Inc. (Website: http://www.photonics.umbc.edu/.)

Heider N. Ereifej, photograph and biography not available at the time of publication.

Vladimir S. Grigoryan, photograph and biography not available at the time of publication.

Gary M. Carter, photograph and biography not available at the time of publication.

Curtis R. Menyuk (SM'88–F'98) was born March 26, 1954. He received the B.S. and M.S. degrees from the Massachusetts Institute of Technology, Cambridge, in 1976 and the Ph.D. degree from the University of California, Los Angeles, in 1981.

He has worked as a Research Associate at the University of Maryland, College Park, and at Science Applications International Corporation, McLean, VA. In 1986, he became an Associate Professor in the Department of Electrical Engineering at the University of Maryland Baltimore County (UMBC), Baltimore, and he was the founding member of the department. In 1993, he was promoted to Professor. He has been on partial leave from UMBC since 1996. From 1996 to 2001, he worked part-time for the Department of Defense (DoD), codirecting the Optical Networking Program at the DoD Laboratory for Telecommunications Sciences, Adelphi, MD, from 1999 to 2001. In August 2001, he left the DoD and became Chief Scientist at PhotonEx Corporation, Maynard MA. For the last 15 years, his primary research interest has been theoretical and computational studies of fiber-optic communications. He has authored or coauthored more than 140 archival journal publications as well as numerous other publications and presentations. He has also edited two books. The equations and algorithms that he and his research group at UMBC have developed to model optical fiber transmission systems are used extensively in the telecommunications industry.

Dr. Menyuk is a Fellow of the Optical Society of America (OSA) and a member of the Society for Industrial and Applied Mathematics and the American Physical Society. He is a former UMBC Presidential Research Professor.

Quantitative experimental study of intra-channel nonlinear timing jitter in a 10 Gb/s terrestrial WDM return-to-zero system

H. Xu, H. Jiao, J. Wen, J. Zweck, L. Yan, C. Menyuk, G. Carter, University of Maryland Baltimore County, Baltimore, MD; G. Carter, The laboratory for Physical Science, College Park, MD.

Abstract:
Using a recirculating loop, we measure nonlinearly-induced timing jitter at different transmission distances for different amounts of pre-compensation. Within each sub-band, we achieve error-free transmission using the same pre-compensation for all channels at all distances up to 5000 km.

Introduction

It is well known that in return-to-zero (RZ) systems, timing jitter induced by nonlinear intra-channel pulse-to-pulse interactions can cause significant performance degradation [1]. It has been shown that in single-span and long-haul point-to-point systems, such as an undersea system, symmetric pre-dispersion compensation at the transmitter and post-dispersion compensation at the receiver minimizes this timing jitter [2]-[5]. In an RZ all-optical terrestrial network, even over short distances, the impact that nonlinearly-induced timing jitter has on the performance is just as important as in a long-haul point-to-point system. However, the problem of optimizing the amount of pre-compensation is more complicated, since different transmission distances require different amounts of pre-compensation to minimize timing jitter and there can be a large variation in the data transmission distance in a network. Moreover, in many terrestrial transmission systems, the accumulated dispersion in each span of transmission fiber can be comparable to the accumulated dispersion in the whole transmission line. Consequently, it is not a trivial task to minimize the impact of timing jitter in a network over the entire range of possible transmission distances.

A first important step required to minimize the effect of nonlinearly-induced timing jitter in an all-optical network is to measure timing jitter as a function of transmission distance, and to assess its impact on the system performance. In this paper, we report measurements of timing jitter as a function of transmission distances up to 5000 km for different amounts of pre-compensation using a recirculating loop that emulates a 10 Gb/s wavelength-division-multiplexed (WDM) terrestrial system with partially slope-compensating inline dispersion-compensation fiber. We present an empirical formula for the optimal pre-compensation as a function of the accumulated span dispersion and accumulated transmission dispersion. We quantify the sensitivity of timing jitter to the transmission distance and the amount of pre-compensation, and we determine its impact on the bit-error rate (BER). Finally, we show that by choosing different fixed amounts of pre-compensation for each 600 GHz-wide sub-band of the C-band we can limit the timing-jitter-induced BER degradation and achieve error-free propagation (BER$<1\times10^{-9}$) simultaneously for all distances up to 5000 km.

Experimental setup

Figure 1 shows our recirculating loop that consisted of four transmission spans of standard single-mode fiber (SMF, D = +17.4 ps/nm-km). Following each transmission span, there was a compensation module that included a dual-stage EDFA and partially slope-compensating

dispersion compensating fiber (DCF, D = – 97 ps/nm-km). The length of transmission fiber in the first and fourth spans was about 50 km and in the second and third spans was about 75 km. The total length of the transmission fiber in the loop, excluding the DCF, was 260 km. We transmitted four equally spaced channels between 1552.6 nm and 1557.4 nm. The relatively wide channel spacing (200 GHz) and large local dispersion helped to minimize inter-channel effects. Gain-flattening filters were used in the loop to compensate the uneven gain profile of the EDFAs. We passed the four channels through an electro-absorption modulator to produce 10 Gb/s return-to-zero pulses with a full-width at half-maximum of 21 ps and then modulated the pulses with a data stream of length 2^{23}–1. The average power per channel was about –2.5 dBm into the SMF and – 6.5 dBm into the DCF.

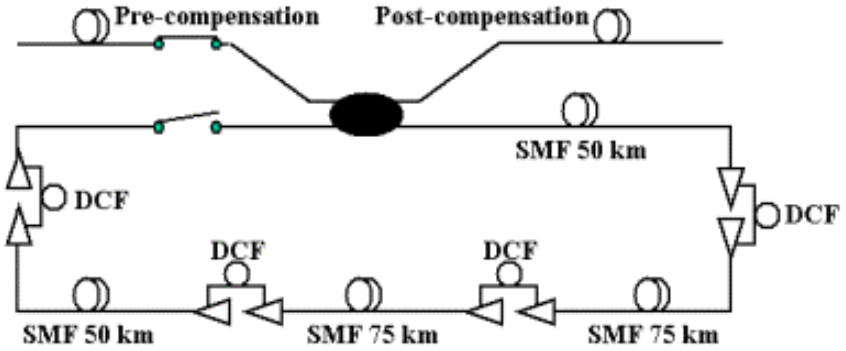

Fig. 1. Schematic diagram of the experimental loop

By varying the average loop dispersion with a short piece of SMF or DCF, we used the four fixed-wavelength channels to study the behavior of different sub-bands in the C-band, which is equivalent to shifting the wavelengths in a fixed dispersion map. In this experiment, we focused on three cases for which the average loop dispersion of channel 4 was –0.29, 0.02, and +0.33 ps/nm-km respectively. These three cases, which we call the D_{-}, D_0, and D_{+} cases, correspond to the short, central, and long wavelength regions of the C-band in which the central wavelength channel experiences zero average transmission dispersion. The average dispersion slope of the loop was around +0.017 ps/nm^2-km. We used an Agilent sampling oscilloscope to record the standard deviation of the timing shift, and an Anritsu bit error rate tester in burst mode to measure the BER. We also measured the optical signal-to-noise ratio using an Agilent optical spectrum analyzer with a resolution bandwidth of 0.2 nm.

Results and discussion

Figure 2 shows the measured timing jitter for channel 4 at 1557.4 nm for each dispersion case. For each timing jitter measurement, we chose the amount of post-compensation to optimize the bit-error rate. Most of the timing jitter comes from the intra-channel nonlinear pulse interactions.

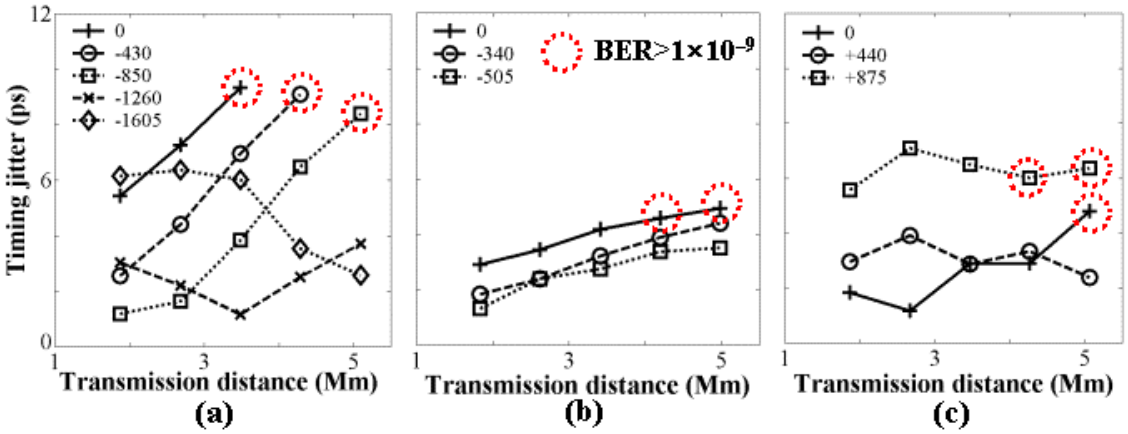

Fig. 2. Timing jitter versus transmission distance for various amounts of pre-compensation (shown in insets with units of ps/nm). (a) Case D_+; (b) Case D_0; (c) Case D_-.

Our measurement results show that the optimal amount of pre-compensation $D_{pre,opt}$ required to minimize the timing jitter varies significantly for different transmission distances and different channels in a terrestrial WDM system. Specifically, $D_{pre,opt}$ depends on both the dispersion accumulated in each span of transmission fiber, D_{span}, and on the accumulated dispersion in the whole transmission line, D_{tran}, and obeys the modified symmetric rule $D_{pre,opt} = -(D_{span}+D_{tran})/2$.

In our loop, the average accumulated span dispersion D_{span} is around +1164 ps/nm for all channels. In Fig. 3, we compare the calculated and the measured optimal amounts of pre-compensation. In all three cases, the calculated values are in reasonably good agreement with the measured values. This formula also applies to the previously studied single span and undersea systems [2-5].

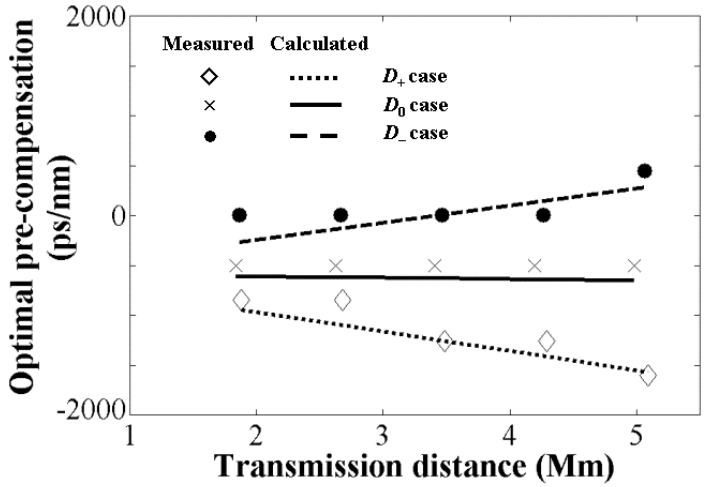

Fig. 3. Comparison of the measured and calculated optimal amounts of pre-compensation.

In a terrestrial system, the sign of the accumulated span dispersion is the same for all channels. However, without ideal dispersion-slope-compensating DCF, different channels have different accumulated transmission dispersion D_{tran}. When D_{tran} has the same sign as D_{span}, as for the D_+ case in Fig. 2a, we need a large amount of pre-compensation to minimize the nonlinearly-induced timing jitter, and this amount increases with distance. For a channel for which D_{tran} has

the opposite sign to D_{span}, as for the D_- case shown in Fig. 2c, the first span of transmission fiber acts as a piece of pre-compensating fiber, and a smaller amount of pre-compensation is needed. When the inline DCF perfectly compensates the accumulated span dispersion, as for the D_0 case shown in Fig. 2b, the optimal amount of pre-compensation does not vary with distance and is mostly determined by D_{span}. This optimal amount of pre-compensation minimizes the timing jitter induced in a single span and consequently the growth rate of timing jitter over distance. At 5000 km, if the amount of pre-compensation deviates from the optimum by about 800 ps/nm in the D_+ case and 400 ps/nm in the D_- case, the timing jitter increases from 2.6 ps to 8.4 ps and from 2.4 ps to 6.4 ps respectively. These large amounts of timing jitter dominate the system performance and prevent the error-free propagation out to this distance.

In Fig. 2, we also observe that, although the system is vulnerable to timing jitter impairments at longer distances, at shorter distances it can tolerate a larger amount of timing jitter. The reason is that amplified spontaneous emission (ASE) noise and nonlinear effects are two of the major limitations for the terrestrial transmission. With smaller ASE noise, the system can tolerate more nonlinearly-induced degradation. Consequently, at 2700 km where the optical signal-to-noise ratio is around 15.0 dB, the system is still error free even when the timing jitter is as large as 7.3 ps, but at 5000 km where the optical signal-to-noise ratio is around 12.0 dB, error-free propagation is not possible with a timing jitter of 4.8 ps. In the D_0 case without pre-compensation, the tolerance to timing jitter is further reduced by self-phase modulation effects, since in each span the pulses are compressed at the input to the SMF, where the average optical power is largest. However, the optimal pre-compensation required to minimize the timing jitter in each span also reduces self-phase modulation effects, since the pulses are broader at the SMF input.

In all-optical networks the data transmission distance can vary dynamically. Our measurements show that for those channels with non-zero transmission dispersion, one can use a fixed pre-compensation configuration that minimizes the nonlinearly-induced timing jitter at a longer distance to achieve low BER over a wide range of distances. For the channels with near-zero transmission dispersion, a fixed amount of pre-compensation can also reduce the timing jitter and SPM effects at all distances. For the system we studied, with a fixed pre-compensation of –1260 or –1605 ps/nm in the D_+ case, –340 or –505 ps/nm in the D_0 case, and +440 ps/nm in the D_- case, we achieved error-free propagation at all distances up to 5000 km across the 600 GHz-wide sub-band. While we still needed to adjust the amount of post-compensation to reduce the waveform distortion induced by residual dispersion and self-phase modulation, using a fixed amount of pre-compensation for a sub-band is a first step to alleviate the complexity of the dispersion compensation in an all-optical network.

Conclusion

Using a recirculating loop we measured timing jitter in a 10 Gb/s WDM terrestrial system and quantified its sensitivity and impact on the BER as a function of transmission distance up to 5000 km for different channels and different amounts of pre-dispersion compensation. We obtained an empirical formula for the optimal pre-dispersion compensation as a function of the accumulated span dispersion and accumulated transmission dispersion. We showed that for an appropriate fixed amount of pre-compensation for each 600 GHz-wide sub-band, error-free transmission can be simultaneously achieved for all distances up to 5000 km.

References

1. P. V. Mamyshev and N. A. Mamysheva, *Opt. Lett.* 24, pp. 1454–1456, (1999).
2. J. Martensson, A. Berntson, M Westlund, A. Danielsson, P. Johannisson, D. Anderson, and M. Lisak, *Opt. Lett.* 26, pp. 55–57, (2001).
3. A. Mecozzi, C. B. Clausen, M. Shtaif, S. G. Park, and A. H. Gnauck, *Photon. Technol. Lett.* 13, pp. 445–447, (2001).
4. E. A. Golovchenko, A. N. Pilipetskii, and N. S. Bergano, *OFC/IOOC'2000*, Baltimore, MD, Mar. 2000, paper FC3.
5. R.-M. Mu and C. R. Menyuk, *Photon. Technol. Lett.* 13, pp. 797–799, (2001).

The Need for Dynamic Control in High Data-Rate Communication Systems

By Gary M. Carter, Professor
CSEE Department, UMBC, Baltimore, MD and
Laboratory for Physical Sciences, 8050 Greenmead Drive, College Park, MD

High data rate optical communication systems will require dynamic control to maintain low error rates for operational systems. The transmission impairments that lead to variable system performance are polarization effects, dispersion, noise, and optical nonlinearity. The polarization effects include polarization dependent loss (PDL), polarization mode dispersion (PMD), and polarization dependent gain (PDG). In many cases these impairments combine to lead to overall system performance degradation. Of particular interest are optical communication networks that will be connected via optical switches. Here one anticipates that high capacity networks of various designs may be optically connected. One may optimize data format, dispersion compensation, and power variation on a given network to achieve good communication performance, but this optimization will in general be different on different networks. One may have to dynamically re-optimize transmission as the two networks are optically connected.

The nonlinear interaction between adjacent pulses in a high data rate channel [1] and the nonlinear interaction between adjacent channels can lead to severe timing jitter even over relatively short distances. Terrestrial WDM systems using only partially dispersion slope compensating (DCF) are particularly susceptible to this problem. Some wavelengths may be near zero total dispersion for the transmission distance while others will accumulate dispersion. The accumulated dispersion can be compensated for in the receiver. As shown in Fig. 1 the accumulated dispersion dramatically affects the timing jitter.

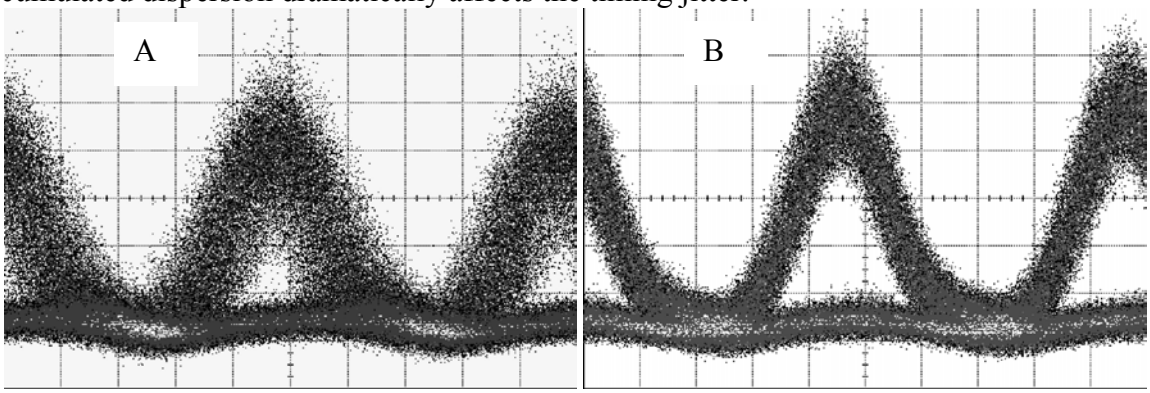

Figure 1. Eye diagrams for 10 Gb/s laboratory loop transmission experiments for a total transmission distance of 3400 km. Figure A has a different accumulated dispersion than Figure B. In both cases the accumulated dispersion is compensated for in the receiver.

This effect can manifest itself in optically switched networks. We have optically connected a Metro network that contains uncompensated standard fiber with a long-haul network. Figure 2 shows eye diagrams for 10 Gb/s transmission experiment on these connected networks for a transmission distance of about 400 km. The accumulated dispersion in this experiment was approximately 800 ps/nm. Figure 2A shows the result for compensating all of the accumulated dispersion at the transmitter. Considerable timing jitter and a low bit-error rate of 1×10^{-7} of was

measured. By splitting the 800 ps/nm between the transmitter and the receiver we obtained the eye in 2B with a bit-error rate of 1×10^{-10} .

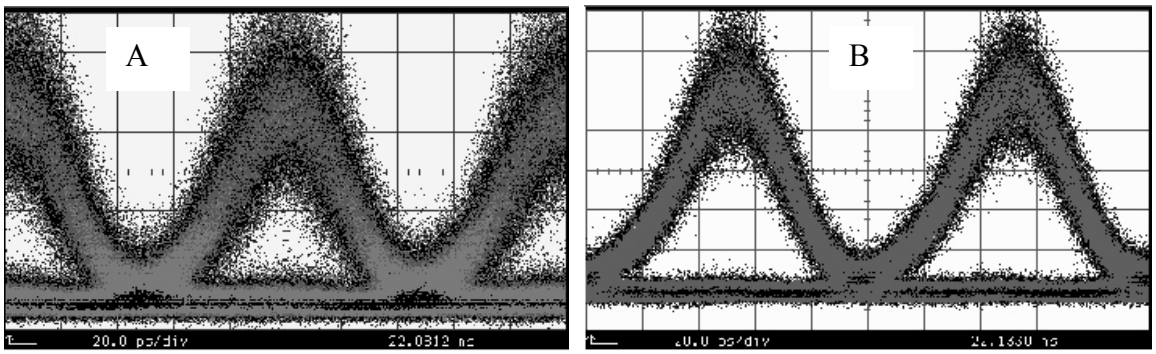

Figure 2. "Eye diagrams for 10 Gb/s experiments over two optically connected networks. The total transmission distance is approximately 400 km. Figure A has all of the residual compensating fiber at the input and B has it split evenly between the input and output.

Polarization also plays in important role in networks as well. In WDM networks amplifiers, multiplexers and demultiplexers have polarization dependent loss (PDL). Figure 3 shows a Q distribution for slow random variation of polarization in a recirculating loop[2]. This variation is due to PDL in the loop. The Q is measured after 5,000 km. This distribution can be drastically altered by the orientation of the fibers. Similar behavior can be expected in networks where the optical signals pass through a number of elements with PDL. Clearly dynamic variation in the fibers can lead to dynamic Q variation. Also polarization mode dispersion (PMD) can have a pronounced effect on system performance. Experimental data will be presented for dynamic PMD measurements taken on an installed network. The results show the need for dynamic PMD compensation on installed networks.

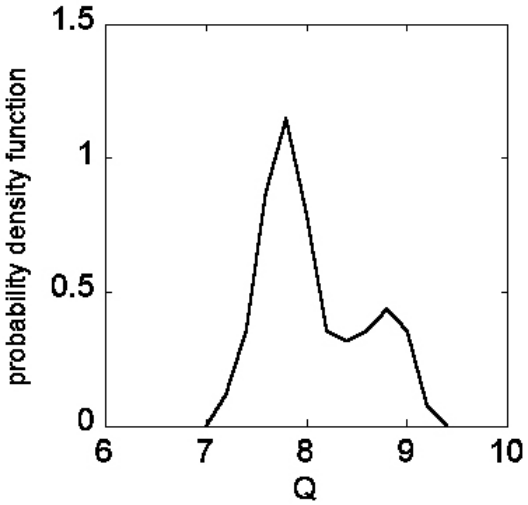

Figure 3. Q distribution for a random polarization variation in a 10 Gb/s loop experiment.

References:

1. P. V. Mamyshev and N. A. Mamysheva, "Pulse-overlapped dispersion-managed data transmission and intrachannel four-wave mixing", Optics Lett. Vol. 24, pp. 1454-1456 (1999).
2. Yu Sun, Ivan T. Lima Jr., Hua Jiao, Jiping Wen, Hai Xu, Heider Ereifej, Gary M. Carter, and Curtis R. Menyuk "Study of system performance in a 107 km dispersion managed recirculating loop due to polarization effects", IEEE, Photonics Technology Letters, Vol. 13, pp. 966-968 (2001).